bioRxiv preprint doi: https://doi.org/10.1101/2020.08.07.241190; this version posted August 7, 2020. The copyright holder for this preprint (which was not certified by peer review) is the author/funder, who has granted bioRxiv a license to display the preprint in perpetuity. It is made available under aCC-BY 4.0 International license.

1 # Amoeba predation of *Cryptococcus neoformans* results in pleiotropic
2 changes to traits associated with virulence

3 Man Shun Fu[1], Livia C. Liporagi-Lopes[1, 2], Samuel R. dos Santos Júnior[1,3], Jennifer L. Tenor[4],
4 John R. Perfect[4], Christina A. Cuomo[5], Arturo Casadevall[1]

5 [1] Department of Molecular Microbiology and Immunology, Johns Hopkins Bloomberg School of
6 Public Health, Maryland, USA.

7 [2] Departamento de Análises Clínicas e Toxicológicas, Faculdade de Farmácia, Universidade
8 Federal do Rio de Janeiro, Rio de Janeiro, Brazil.

9 [3] Departamento de Microbiologia, Instituto de Ciências Biomédicas, Universidade de São Paulo,
10 São Paulo, Brazil.

11 [4] Division of Infectious Diseases, Department of Medicine and Department of Molecular
12 Genetics and Microbiology, Duke University, North Carolina, USA.

13 [5] Infectious Disease and Microbiome Program, Broad Institute, Cambridge, Massachusetts, USA.

14 [*]Address correspondence to: Arturo Casadevall, M.D., Ph.D.
15 Johns Hopkins Bloomberg School of Public Health
16 615 N Wolfe St
17 Baltimore, MD 21205
18 Telephone: (410) 955-3459
19 Fax: (410) 502-5884
20 Email: acasade1@jhu.edu

21

22 Running title: Amoeba predation of *C. neoformans* results in pleiotropic traits

23

bioRxiv preprint doi: https://doi.org/10.1101/2020.08.07.241190; this version posted August 7, 2020. The copyright holder for this preprint (which was not certified by peer review) is the author/funder, who has granted bioRxiv a license to display the preprint in perpetuity. It is made available under aCC-BY 4.0 International license.

24 **Abstract**

25 **Phagocytic amoeboid predators such as amoeba have been proposed to select for survival**
26 **traits in soil microbes such as *Cryptococcus neoformans* that can also function in animal**
27 **virulence by defeating phagocytic immune cells, such as macrophages. Several prior studies**
28 **have shown that incubation of various fungal species with amoeba can enhance their**
29 **virulence. However, the mechanisms by which fungi adapt to amoeba and thus change**
30 **their virulence are unknown. In this study we exposed three strains of *C. neoformans* (1**
31 **clinical and 2 environmental) to predation by *Acanthamoeba castellanii* for prolonged**
32 **periods of time and then analyzed surviving colonies phenotypically and genetically.**
33 **Surviving colonies were comprised of cells that expressed either pseudohyphal or yeast**
34 **phenotypes, which demonstrated variable expression of such traits associated with**
35 **virulence such as capsule size, urease production and melanization. Phenotypic changes**
36 **were associated with aneuploidy and DNA sequence mutations in some amoeba-passaged**
37 **isolates, but not in others. Mutations in the gene encoding for the oligopeptide transporter**
38 **(CNAG_03013; *OPT1*) were observed among amoeba-passaged isolates from each of the**
39 **three strains. In addition, isolates derived from environmental strains gained the capacity**
40 **for enhanced macrophage toxicity after amoeba selection and carried mutations on the**
41 **CNAG_00570 gene, which encodes Pkr1 (AMP-dependent protein kinase regulator) but**
42 **were less virulence in mice because they elicited more effective fungal-clearing immune**
43 **responses. Our results indicate that *C. neoformans* survival under constant amoeba**
44 **predation involves the generation of strains expressing pleiotropic phenotypic and genetic**
45 **changes, which confer increase resistance against protozoal predation. Given the myriad of**
46 **potential predators in soils the diversity observed among amoeba-selected strains suggests**

bioRxiv preprint doi: https://doi.org/10.1101/2020.08.07.241190; this version posted August 7, 2020. The copyright holder for this preprint (which was not certified by peer review) is the author/funder, who has granted bioRxiv a license to display the preprint in perpetuity. It is made available under aCC-BY 4.0 International license.

47 **a bet-hedging strategy whereby variant diversity increases the likelihood that some will**

48 **survive predation.**

49

bioRxiv preprint doi: https://doi.org/10.1101/2020.08.07.241190; this version posted August 7, 2020. The copyright holder for this preprint (which was not certified by peer review) is the author/funder, who has granted bioRxiv a license to display the preprint in perpetuity. It is made available under aCC-BY 4.0 International license.

50 **Author summary**

51 *Cryptococcus neoformans* is a ubiquitous environmental fungus that is also a leading cause of
52 fatal fungal infection in humans, especially among immunocompromised patients.
53 Cryptococcosis is a worldwide concern due to its high mortality rate. A major question in the
54 field is how an environmental yeast such as *C. neoformans* becomes a human pathogen when it
55 has no need for animal host in its life cycle. Previous studies showed evidence that *C.*
56 *neoformans* increases its pathogenicity after interacting with its environmental predator
57 amoebae. Amoebae behave like macrophages, an important immune cell in human body, so it is
58 considered as a training ground for pathogens to resist macrophages. However, how *C.*
59 *neoformans* changes its virulence through interacting with amoebae is unknown. Here, we
60 exposed *C. neoformans* to amoebae for a long period of time. We found that *C. neoformans* cells
61 recovered from amoebae manifested numerous changes to phenotypes related to its virulence and
62 one of the amoeba-passaged *C. neoformans* cells had enhanced ability to kill macrophages. We
63 further analyzed their genome sequences and found various mutations in different cells of
64 amoeba-passaged *C. neoformans*, showing that DNA mutations may be the major cause of the
65 phenotypic changes after interacting with amoebae. Our study indicates that fungal survival in
66 the face of amoeba predation is associated with the emergence of pleiotropic phenotypic and
67 genomic changes that increase the chance of fungal survival.

68

bioRxiv preprint doi: https://doi.org/10.1101/2020.08.07.241190; this version posted August 7, 2020. The copyright holder for this preprint (which was not certified by peer review) is the author/funder, who has granted bioRxiv a license to display the preprint in perpetuity. It is made available under aCC-BY 4.0 International license.

69 **Introduction**

70 *C. neoformans* is a major life-threatening fungal pathogen that predominantly infects severely
71 immunocompromised patients and causes over 180,000 deaths per year worldwide [1].
72 C. *neoformans* expresses virulence factors that promote its pathogenicity in humans, including
73 formation and enlargement of a polysaccharide capsule that interferes with the host immune
74 system in varied ways, melanin production that protects against oxidative stress [2–5], and
75 extracellular secretion of various enzymes including phospholipase and urease [6,7]. *C.*
76 *neoformans* is found primarily and ubiquitously in environments such as soils contaminated with
77 bird excreta or from trees [8–11]. It is a saprophyte and does not require an animal host for
78 survival and reproduction. Besides, there is rare evidence of human-to-human transmission and
79 thus it is unlikely that its virulence traits were selected for causing disease in humans or animals.
80 That raises the fundamental question of how *C. neoformans* acquired those traits, which are
81 essential for pathogenesis of cryptococcosis in human.

82 A hypothesis to solve this enigma is that of coincident selection, resulting from selective
83 pressures in both natural environmental and animal niches such as predatory amoeba and
84 nematodes [12]. According to this view, microbial traits selected for environmental survival also
85 confer the capacity for virulence by promoting survival in animal hosts [12]. For example, the
86 capsule can protect the fungi from desiccation and against predatory amoeba [13,14] while
87 melanin may reduce damage of fungi from the exposure to UV radiation, osmotic stresses or
88 extreme temperatures [15–18]. Urease provides a nutritional role involved in nitrogen acquisition
89 in the environment [19]. Moreover, it is striking that *C. neoformans* isolates from the soil are
90 virulent for animal hosts [20]. Understanding the evolutionary adaption of *C. neoformans* in

bioRxiv preprint doi: https://doi.org/10.1101/2020.08.07.241190; this version posted August 7, 2020. The copyright holder for this preprint (which was not certified by peer review) is the author/funder, who has granted bioRxiv a license to display the preprint in perpetuity. It is made available under aCC-BY 4.0 International license.

91 nature will help us to understand further the origin of virulence and pathogenesis of
92 cryptococcosis.

93 Amoebae are one of the major sources of selective pressure in nature for broad range of soil
94 microorganisms that have pathogenic potential for humans, including bacteria such as *Legionella*
95 *pneumophila*, *Mycobacterium spp* and fungi such as *Cryptococcus neoformans*, *Aspergillus*
96 *fumigatus* and *Paracoccidioides spp* [14,21–24]. Similar to human macrophages, amoebae ingest
97 microorganisms, undergo a respiratory burst, phagosome maturation and acidification, expresses
98 cell surface receptors and expel undigested materials [25–31]. However, many bacteria and fungi
99 have strategies to survive in amoebae, that function in parallel for survival in mammalian
100 phagocytic cells. For example, *L. pneumophila* utilizes similar cellular and molecular
101 mechanisms of invasion, survival and replication inside both amoeba and macrophages [32–37].
102 Amoeba-grown *L. pneumophila* are more invasive for epithelial cells and macrophages [21].
103 After passage in amoeba, *Mycobacterium avium* enhances both entry and intracellular replication
104 in epithelial cells and is more virulent in the macrophage and mouse models of infection [22].
105 Among fungal pathogens, concordance of virulence factor function for amoeba and animals was
106 also demonstrated for *A. fumigatus* [23]. For example, the mycotoxin fumagillin can inhibit the
107 growth of *Entamoeba histolytica* while it can also cause mammalian epithelial cell damage [38].
108 Many studies have been done to explore amoeba-*C. neoformans* interaction, and shown evidence
109 that amoebae influence the virulence of *C. neoformans* for mammalian infection [39,40].
110
111 *Acanthamoeba castellanii* was originally isolated from cultures of a *Cryptococcus* spp., and like
112 other amoebae species preys on *Cryptococcus* spp [41,42]. There is evidence that amoebae are
113 natural predators of *C. neoformans* in the natural environment [43]. On the other hand, *C.*

bioRxiv preprint doi: https://doi.org/10.1101/2020.08.07.241190; this version posted August 7, 2020. The copyright holder for this preprint (which was not certified by peer review) is the author/funder, who has granted bioRxiv a license to display the preprint in perpetuity. It is made available under aCC-BY 4.0 International license.

114 *neoformans* is able to resist the destruction by amoeba, especially in nutrient poor conditions
115 [44] without metal cations [45]. Several studies have shown that the virulence factors and the
116 cellular process that fungi use for defending against amoeba predation are remarkably similar to
117 those employed for mammalian virulence. For example, the capsule formation and melanin
118 production are important for *C. neoformans* to resist predation by *A. castellanii* and play
119 important roles for pathogenicity in mammalian infection [14,39]. Interestingly, the
120 phospholipids that are secreted by both macrophages and amoebae trigger capsule enlargement
121 [40]. The non-lytic exocytosis process which is found in macrophage containing *C. neoformans*
122 can be also observed in *A. castellanii* and *D. discoideum* through the similar action of actin
123 polymerization [46,47]. Transcriptional studies showed a conserved metabolic response of *C.*
124 *neoformans* to the microenvironments of both macrophage and amoebae [48]. All those common
125 strategies found to adapt to both amoebae and macrophages support the hypothesis that
126 cryptococcal pathogenesis is derived from the interaction with amoebae in natural environment.
127 More direct evidence comes from the experiment on the passage of an attenuated cryptococcal
128 strain to *D. discoideum* cultures that shows enhancement of fungal virulence in a murine
129 infection model [39]. Passaged *C. neoformans* also exhibits capsule enlargement and rapid
130 melanization, suggesting that those are mechanisms to enhance the survival of fungus in mice.
131 However, the underlying mechanism on how these phenotypic changes occur is still unclear.

132 In this study, we sought to determine the long-term evolutionary adaption of *C. neoformans*
133 when interacting with amoeba and whether the adaption affected virulence traits for animal
134 hosts. Our results show that persistent amoeba predation was associated with the emergence of
135 pleiotropic phenotypic changes of *C. neoformans.*

136

bioRxiv preprint doi: https://doi.org/10.1101/2020.08.07.241190; this version posted August 7, 2020. The copyright holder for this preprint (which was not certified by peer review) is the author/funder, who has granted bioRxiv a license to display the preprint in perpetuity. It is made available under aCC-BY 4.0 International license.

137 **Result**

138 Selection of amoeba-resistance strains. We studied the interaction between *C. neoformans* and
139 *Acanthamoeba castellanii* by culturing them together on Sabouraud agar. For the initial
140 experiments, we used the well-studied common laboratory strain H99. The experimental setup
141 involved spreading approximately 200 cryptococcal cells on agar followed by placing
142 approximately 5000 *A. castellanii* cells on the plate. After approximately month of co-
143 incubation, small colonies emerged within the predator zone of *A. castellanii* (Fig 1A),
144 sometimes under the mat of amoeba. Microscopic morphological analysis of cells in those
145 colonies revealed pseudohyphal and hyphal forms of *C. neoformans* (Fig 1B & C). We selected
146 20 single hyphal cells from two colonies (ten hyphae from each colony) and these were
147 transferred to a fresh Sabouraud agar plate without amoeba (Fig 1D, E & I). After 24 h,
148 microcolonies composed exclusively of yeast cells emerged on the agar (Fig 1F & J), which
149 manifested two distinct colonies morphologies, smooth and serrated, after two days of agar
150 growth (Fig 1G & K). All of the cells from these colonies were yeasts (Fig 1H & L). The same
151 experiment was then repeated with two environmental avirulent *C. neoformans* strains, A1-35-8
152 and Ftc555-1, but this time total 20 single hyphae were picked from four survival colonies (five
153 hyphae from each colony) to a fresh agar plate. Like the experience with H99, these strains
154 responded to the presence of amoeba by generating cells that formed colonies with various
155 cellular and colony morphologies, of which some (A4-6) were slightly serrated with
156 pseudohyphal cells (Fig 1M). We also observed some hyphal colonies formed by Ftc555-1 cells
157 but eventually they converted back to yeast cells when streaked on fresh agar medium (Fig 1N).
158 The results showed that after interacting with amoebae, *C. neoformans* can develop high variety
159 of cellular and colony morphologies even in amoebae-free medium.

bioRxiv preprint doi: https://doi.org/10.1101/2020.08.07.241190; this version posted August 7, 2020. The copyright holder for this preprint (which was not certified by peer review) is the author/funder, who has granted bioRxiv a license to display the preprint in perpetuity. It is made available under aCC-BY 4.0 International license.

160 Six colonies from each strain were selected together with three controls, which were colonies on
161 the same plate with isolates but without interacting with amoeba, for further phenotypic
162 characterization (Fig 1D). These will be referred heretofore to as amoeba-passaged isolates with
163 numbers preceded by the letters H, A, and F to indicate their origin from strains H99, A1-35-8
164 and Ftc555-1, respectively. Controls will be referred to as C1-3 and ancestor will be referred to
165 as A. To test if amoeba exerts selection pressure that resulted in amoeba-resistant cells, we
166 examined if those isolates increased their survival during amoeba interaction. Isolates were then
167 co-incubated with amoeba in the agar medium again, with *C. neoformans* in a cross, and amoeba
168 were spotted in the center (Fig 2A). The radii of clear zones were measured as a function of time
169 and these represented how well the amoeba clears the culture of *C. neoformans*. All of the
170 amoeba-passaged isolates derived from H99 had reduced size of predator zone, when compared
171 with their controls and ancestor strain (Fig 2B). In particular, the isolates that formed smooth
172 colonies (H13, H16, H17) had the smallest predation zone (Fig 2B). This result implies that
173 amoeba passage resulted in *C. neoformans* strains with increased ability to subsequently resist
174 predation by amoeba. Next, we investigated the mechanism of the resistance. Samples were
175 taken at the edge of the predator zone at the early stage of the interaction (week one), and
176 observed under microscope. Isolates H13, H16 and H17 formed pseudohyphae while most of the
177 cells in isolates H1, H2, H14 were in yeast form, with some displaying pseudohyphae (Fig 2C).
178 However, no pseudohyphae were found in cells from controls and H99 ancestor colonies
179 although pseudohyphae were formed eventually at the late stage of the interaction. Samples were
180 also taken at a distance from the predation zone where cryptococcal cells had no contact with
181 amoebae and in each of these regions all cells were in yeast form (Fig 2D). These results showed
182 that pseudohyphal cells emerged rapidly from each of the amoeba-passaged strains even thought

bioRxiv preprint doi: https://doi.org/10.1101/2020.08.07.241190; this version posted August 7, 2020. The copyright holder for this preprint (which was not certified by peer review) is the author/funder, who has granted bioRxiv a license to display the preprint in perpetuity. It is made available under aCC-BY 4.0 International license.

183 their cells were yeast prior to the incubation with amoebae and that pseudohyphal formation is a
184 major mechanism of increased ability to resist predation.

185 When the isolates derived from A1-35-8 and Ftc555-1 strains were again exposed to *A.*
186 *castellanii*, some but not all exhibited increased resistance to amoebae (Fig 3A & B). Isolates
187 derived from A1-35-8 (A4-6) were significantly more resistant than the others (Fig 3A). That
188 may be due to maintenance of pseudohyphal cell morphology by isolates A4-6 even in the
189 amoebae-free medium. Isolates F3-5 manifested increased resistance to amoeba but unlike the
190 H99 derived isolates, displayed no pseudohyphal formation but had larger cells when compared
191 to their ancestor (Fig 3C & D) at the early stage of interaction, which may be another survival
192 strategy for *C. neoformans* against amoebae. In this regard, phagocytosis of *C. neoformans* by
193 macrophage was reduced by cell enlargement of *C. neoformans* [49–51]. The resistance of
194 isolates F3-F5 to amoebae may reflect their larger cell size.

195 Effects of amoeba selection on known virulence factors. *C. neoformans* expresses virulence
196 factors that promote its pathogenicity, including formation and enlargement of a polysaccharide
197 capsule, melanin production, extracellular secretion of urease, and cell enlargement. To evaluate
198 whether the emergence of variant form of *C. neoformans* was accompanied by changes to known
199 virulence factors, we analyzed the virulence-related phenotypic characteristics of the isolates
200 derived from the three strains. Isolates H13, H16 and H17 had larger capsule thickness relative to
201 their ancestor when cultured in minimal medium but cell sizes were similar (Fig 4A and 5A). All
202 of the isolates also had increased urease activity in comparison to their ancestor (Fig 6). Isolates
203 H1, H2 and H14 manifested less melanin production (Fig 7). We also examined if there were
204 any changes of virulence factors in isolates of environmental strains. Each of the isolates derived
205 from A1-35-8 strain had increased capsule size, reduced melanin production and increased

bioRxiv preprint doi: https://doi.org/10.1101/2020.08.07.241190; this version posted August 7, 2020. The copyright holder for this preprint (which was not certified by peer review) is the author/funder, who has granted bioRxiv a license to display the preprint in perpetuity. It is made available under aCC-BY 4.0 International license.

206 urease activity when comparing to their ancestor, but there was no change in cell size (Fig 4B,
207 5B and 6). Isolates F3-F6 has increased both their capsule and cell size in minimal medium (Fig
208 4C and 5C). They were also having 15-18% of cells with size larger than 10 μm inside
209 macrophages (Fig 5E) while approximately 80% of cells with larger than 10 μm in macrophage
210 medium in 37°C 9.5% $CO_2$ (Fig 5D). Moreover, all of the isolates of Ftc555-1 strain had
211 increased urease activity, but reduced melanin production (Fig 6 and 7).

212 We further characterized the isolates in stress conditions by analyzing their growth under thermal
213 stress and exposure to the antifungal drug fluconazole (Fig 8). Isolates H13, H16, H17 had
214 reduced growth at 40°C and in the presence of fluconazole while H1, H2 and H14 had slightly
215 increased their resistance to fluconazole compared to their ancestral strain. Isolates A4-A6 and
216 F3-F6 displayed defects in growth at high temperature and after exposure to fluconazole.

217 Overall, the data show that the phenotypic changes were broad and diverse among isolates.

218 <u>Genomic analysis and sequencing results.</u> A prior study showed that DNA mutation was
219 involved in pseudohyphal formation during amoebae interaction [52]. To find out if there are any
220 such mutations or any other mutations in our experiments, the genomes of all isolates were
221 sequenced. SNPs and indels were identified compared to the H99 reference genome (Table 1, 2
222 and table in S1 table). Genome sequencing revealed that H and A isolates acquired only a small
223 number of SNPs and indels during amoeba passage, whereas F isolates acquired an order of
224 magnitude more SNPs and indels. Two SNPs were identified in H1, H2, H14 in comparison with
225 their ancestral strain H99. One of the SNPs is a missense mutation (M484R) in a gene encoding
226 an oligopeptide transporter (CNAG_03013; *OPT1*). This mutation creates the replacement of
227 methionine 484 with arginine. Opt1 has been shown to be required for transporting Qsp1, a
228 quorum sensing peptide, into the receiving cells [53]. Another SNP is an intron variant in a gene

bioRxiv preprint doi: https://doi.org/10.1101/2020.08.07.241190; this version posted August 7, 2020. The copyright holder for this preprint (which was not certified by peer review) is the author/funder, who has granted bioRxiv a license to display the preprint in perpetuity. It is made available under aCC-BY 4.0 International license.

229 encoding a protein kinase (CNAG_02531; *CPK2*) as part of the MAPK protein kinase family.
230 Loss of CPK2 reduces melanin production in Niger seed media. For A1-35-8 derived isolates, a
231 total of four SNPs were identified relative to the ancestral strain A1-35-8. In A1, one missense
232 SNP was found in CNAG_01101, which encodes a hypothetical protein with a centrosomin N-
233 terminal motif and also a single nucleotide deletion was identified in CNAG_03013, causing a
234 frameshift at P358. Two SNPs were identified in A2 and A3 isolates, with one SNP leading to
235 nonsense mutation in CNAG_03013 and another SNP resulting in missense mutation in
236 CNAG_02858 which encodes adenylsuccinate synthetase. Another SNP in the A2 isolate was
237 found in an intergenic region, a site with a high fraction of ambiguous calls. Isolates A4-6 had a
238 single nucleotide deletion at gene CNAG_03622 (*TAO3*) and leads to the frameshift at residue
239 150 of 2392. This mutation is consistent to the finding in previous study that *TAO3* mutation lead
240 to the pseudohyphal phenotype [52]. In contrast to the A1-35-8 isolates, the rate of mutations in
241 the Ftc555-1 isolates was 10 times higher, ranging from 22 to 77 SNPs (total 225 SNPs) and 7-
242 15 indels (total 34 indels) in these isolates. Among those SNPs, three SNPs were annotated as
243 high impact mutations resulting in disruption of the coding region (early stop codons and splice
244 site mutations). One SNP results in a nonsense mutation (G407*) in CNAG_00570 which
245 encodes Pkr1 (AMP-dependent protein kinase regulator) in F5 and F6 isolates. In addition, F3
246 and F4 isolates carry a single nucleotide deletion in CNAG_00570 leading to frameshift of
247 residues 194 of 482. Pkr1 is one of the important components of cAMP/PKA pathway and
248 negatively regulates Pka activity which is involved in morphogenesis, nutrient acquisition, stress
249 responses and virulence in *C. neoformans* (Choi et al., 2012). Another SNP in the F1 isolate is a
250 splice site mutation in CNAG_03013. In summary, there are three noteworthy observations in
251 the sequence data: 1. The gene CNAG_03013 (*OPT1*) was impacted by non-synonymous SNP

bioRxiv preprint doi: https://doi.org/10.1101/2020.08.07.241190; this version posted August 7, 2020. The copyright holder for this preprint (which was not certified by peer review) is the author/funder, who has granted bioRxiv a license to display the preprint in perpetuity. It is made available under aCC-BY 4.0 International license.

252 changes in all three strain backgrounds; 2. The previously described *TAO3* mutation responsible
253 for pseudohyphal or hyphal formation was found in our isolates A4, A5, A6 [52]; and, 3. No
254 SNPs and indels were found in some of the isolates including H13, H16, H17 suggesting that the
255 phenotypic changes observed did not originate from single nucleotide variants in the genome.

256 **Table 1. High and moderate impact SNPs found in passaged isolates**

| Isolates | Chr | Position | Reference | Alternate | Gene ID | Gene function | Effect of mutation |
|---|---|---|---|---|---|---|---|
| H1, H2, H14 | 3 | 211613 | T | G | CNAG_03013 | Oligopeptide transporter | M484R |
| H1, H2, H14 | 6 | 68953 | C | A | CNAG_02531 | Calcium-dependent protein kinase | Intron variant |
| A1 | 5 | 1208219 | T | C | CNAG_01101 | Hypothetical protein | R478G |
| A2, A3 | 3 | 213165 | G | A | CNAG_03013 | Oligopeptide transporter | Nonsense mutation W932* |
| A2, A3 | 3 | 594765 | A | G | CNAG_02858 | Adenylsuccinate synthetase | I346V |
| A2 | 13 | 592173 | C | T | | Intergenic region | |
| F1[†] | 3 | 213566 | G | T | CNAG_03013 | Oligopeptide transporter | Splice site mutation |
| F5, F6[†] | 1 | 1469244 | C | A | CNAG_00570 | cAMP-dependent protein kinase regulator | Nonsense mutation G407* |
| FC2[†] | 11 | 136455 | T | G | CNAG_01506 | Hypothetical protein | Splice site mutation |

257 [†] Only high impact mutations of Ftc555-1 variants were shown in this table.

258 **Table 2 High impact indels found in passaged A1-35-8 isolates**

| Isolates | Chr | Position | Reference | Alternate | Gene ID | Gene function | Effect of mutation |
|---|---|---|---|---|---|---|---|
| A1 | 3 | 211137 | GC | G | CNAG_03013 | Oligopeptide transporter | Frameshift at P358 |
| A4, A5, A6 | 2 | 363200 | CA | C | CNAG_03622 | Cell polarity | Frameshift at N150 |

259

bioRxiv preprint doi: https://doi.org/10.1101/2020.08.07.241190; this version posted August 7, 2020. The copyright holder for this preprint (which was not certified by peer review) is the author/funder, who has granted bioRxiv a license to display the preprint in perpetuity. It is made available under aCC-BY 4.0 International license.

260 To determine if the high impact mutations we identified in genes *PKR1*, *OPT1*,
261 CNAG_02531 and CNAG_01506 are responsible for resistance to the killing of amoebae,
262 deletion mutants of the candidate genes in the H99 background were co-incubated with amoebae
263 on solid medium. However, the predator zones from these mutants were comparable with the
264 parental strain (S2 Fig).

265 Aneuploidy. We next hypothesized that emergence of aneuploidy could be a source of
266 evolutionary adaptation because aneuploidies are frequent in *C. neoformans* and it has been
267 shown to play crucial roles in stress resistance [54,55]. To this end, the chromosomal copy
268 numbers of the isolates were defined based on the normalized depth of sequence coverage. The
269 analysis revealed that there were duplications of chromosome 8 in isolates H13, H16 and H17,
270 but no chromosomal duplication has been found in other isolates (Fig 9A). The results were
271 confirmed by qPCR with two selected isolates, H14 and H17 (Fig 9B and S1 Fig). We next
272 investigated if this chromosomal duplication was responsible for the pseudohyphal formation
273 and other phenotypic changes. In order to do so, H17 was passaged in fresh rich medium every
274 day for 30 days to eliminate the duplication. The elimination was confirmed by qPCR (Fig 9C).
275 H17 euploid strain ($H17^{eu}$) was then co-incubated with amoebae culture in solid medium, and
276 samples were taken from the edge of the predation zone and visualized under microscope. No
277 pseudohyphae could be observed in $H17^{eu}$ (Fig 9D). In such case, the observation was similar to
278 what we found in H99, but distinct from H17 aneuploid strain ($H17^{aneu}$) that forms mostly
279 pseudohyphae after one-week co-incubation (Fig 9D). Not surprisingly, $H17^{eu}$ had decreased
280 ability for amoebal resistance, having a similar size of the predator zone as H99 while $H17^{aneu}$
281 had a smaller predator zone (Fig 9E). The capsule size of $H17^{eu}$ was smaller than $H17^{aneu}$ and
282 similar to H99, suggesting that the duplication of chromosome 8 results in larger capsule size

bioRxiv preprint doi: https://doi.org/10.1101/2020.08.07.241190; this version posted August 7, 2020. The copyright holder for this preprint (which was not certified by peer review) is the author/funder, who has granted bioRxiv a license to display the preprint in perpetuity. It is made available under aCC-BY 4.0 International license.

283 (Fig 9F). H17$^{eu}$ had lower urease activity than H17$^{aneu}$ but comparable level with H99 after 1 h
284 (Fig 9G). However, the urease activity of H17$^{eu}$ increased faster than that of H99 after 1.5 h.
285 The result implied that the chromosomal duplication may be responsible partially the high urease
286 activity found in H17$^{aneu}$.

287 Aneuploidy can arise from multinucleate state through transient polyploidization after
288 failed cytokinesis or cell fusion. The filamentous multinucleate fungus *Ashbya gosypii* exhibits
289 both polyploidy and aneuploidy frequently after cell division [56]. Since pseudohyphae have a
290 cytokinesis defect and multinuclei within a common cytosol, we asked if the pseudohyphal
291 formation may lead to ploidy variation and thus may become one of the sources of phenotypic
292 variation. Consequently, H99 expressing green fluorescent protein-labeled histione-2 (GFP-H2B)
293 were visualized by time-lapsed imaging, and a nucleus fusion have been observed in one of the
294 pseudohyphae after nuclei separation (Fig 10 & S1 Movie). This event provides evidence that
295 polyploidization can exist in pseudohyphae and thus may have a high chance of leading to
296 aneuploidy and phenotypic variation.

297 Epigenetic modifications. Chromatin remodeling can rapidly moderate transcriptional response
298 in order to let the microorganism to adapt rapidly to stressful conditions in hosts. Histone
299 acetyltransferase activity has been shown to be essential for *C. neoformans* in virulence
300 regulation and response to host environments [57]. Since the phenotypes changed rapidly after *C.*
301 *neoformans* interacted with amoebae, we hypothesized that histone acetylation may be involved
302 in the phenotypic changes. To determine whether the evolution of *C. neoformans* after
303 interacting with amoebae also involved histone modification, we compare the quantitation of the
304 acetylation of core histone H3. However, we did not detect significant differences in global
305 histone H3 acetylation between isolates and ancestral strains (S3 Fig).

bioRxiv preprint doi: https://doi.org/10.1101/2020.08.07.241190; this version posted August 7, 2020. The copyright holder for this preprint (which was not certified by peer review) is the author/funder, who has granted bioRxiv a license to display the preprint in perpetuity. It is made available under aCC-BY 4.0 International license.

306 Effects of amoeba selection on interactions with murine macrophages. Based on the changes of
307 multiple virulence-related phenotypes, we expected that some of the isolates would have a better
308 survival when interacting with macrophages. However, there was no significant change of
309 intracellular survival among all the isolates (Fig 11A-C). Nevertheless, we cannot rule out the
310 possibility that isolates may cause damage to macrophages. Since isolates F3-F6 underwent cell
311 enlargement inside macrophage, we hypothesis the increased cell size may physically rupture
312 macrophages. Therefore, we measured the release of lactate dehydrogenase (LDH) from the
313 macrophage when they were infected with Ftc555-1 isolates. Indeed, it was found that LDH
314 release was significantly induced from the macrophages containing F3-F6 when compared to the
315 ancestral strain (Fig 11D), suggesting that F3-F6 and their enlarged yeast cells cause certain
316 damages to their host cells.

317 Virulence testing in murine model and moth larvae. The deletion of PKR1 has been reported to
318 be manifest hypervirulence in mice infection [58]. Since isolates F5 and F6 were more cytotoxic
319 to macrophages and contained loss of function mutations in *PKR1*, we investigated the virulence
320 of F5 and F6 and their parental strain Ftc555-1 in a murine infection model. However, all
321 animals survived after intranasal inoculation for 60 days (data not shown). Lung fungal burden
322 was determined by enumerating CFU. Only the cells of the initial isolate (Ftc555-1) were
323 detected in the mouse lung after this incubation period and there was considerable mouse-to-
324 mouse variation in CFU. Hence, the two isolates carrying *PKR1* mutations were cleared from the
325 lungs 60 days after inoculation (Fig 12). Consequently, we explored early times of infection and
326 noted that at day 5 after challenge both Ftc555-1 and F5 had comparable fungal burden while
327 that of F6 was reduced (Fig 12). To determine if the different proliferation rates of the strains are
328 the reason of the fungal burden difference, proliferation analysis were performed to observe the

bioRxiv preprint doi: https://doi.org/10.1101/2020.08.07.241190; this version posted August 7, 2020. The copyright holder for this preprint (which was not certified by peer review) is the author/funder, who has granted bioRxiv a license to display the preprint in perpetuity. It is made available under aCC-BY 4.0 International license.

329 growth curves of the three *C. neoformans* strains. Two growth curves were prepared in similar
330 conditions, except the initial number of yeasts. Starting the curve with a high concentration of
331 cells ($1.0x10^7$) displayed a similar growth increase for F5 and F6 cells during the first 36 hours,
332 but the very opposite was observed when the curve started with a low concentration of cells
333 ($5.0x10^3$), with a higher growth increase for Ftc555-1 strain (S4 Fig). Hence, all three strains
334 were able to establish themselves in mice initially and survive clearance by innate immunity but
335 the F5 and F6 were subsequently cleared, presumably by the development of acquired immunity.

336 To gain more insight into the immune responses elicited by Ftc555-1, F5 and F6 in the lung
337 we studied several cytokine responses. In the lungs, the levels of pro-inflammatory cytokines,
338 including tumor necrosis factor alpha (TNF-$\alpha$) and interferon gamma (IFN-$\gamma$), were increased and
339 remained high after the 60 d post-infection with F5 and F6 strains (Fig 12). The lung cytokine
340 response shows that F5 and F6 elicit lower levels of IL-10 than Ftc555-1, which could help their
341 clearance from lung tissue relative to Ftc555-1 since reduction of this anti-inflammatory cytokine
342 has been associated with increased resistance to cryptococcal infection in mice [59]. Interestingly,
343 the levels of the same molecules were different when we analyzed the systemic immune response
344 as measured by cytokines in their spleens (S5 Fig). These results may indicate that sustaining high
345 levels of these cytokines may stimulate an inflammatory reaction, which could be associated with
346 resolution of the infection of the mutant strains. These cytokine results show that Ftc555-1 is
347 eliciting quantitatively different immune responses from the parent strain Ftc555-1 consistent with
348 the notion that the differences in virulence observed for these strains reflect differences in the
349 effectiveness of the immune responses triggered.

350 We also examine the virulence of the isolates using wax moth larvae model, and isolates
351 H13, H16 and H17 were less virulence than their ancestor (S6A Fig). This may due to the fact

bioRxiv preprint doi: https://doi.org/10.1101/2020.08.07.241190; this version posted August 7, 2020. The copyright holder for this preprint (which was not certified by peer review) is the author/funder, who has granted bioRxiv a license to display the preprint in perpetuity. It is made available under aCC-BY 4.0 International license.

352 that these isolates can form pseudohyphae rapidly in the larvae, and pseudohyphal *C.*
353 *neoformans* are attenuated for virulence in wax moth larvae [52]. However, so far, there was no
354 statistically significant increased virulence of isolates in the wax moth larvae infection model (S6
355 Fig).

356

357

bioRxiv preprint doi: https://doi.org/10.1101/2020.08.07.241190; this version posted August 7, 2020. The copyright holder for this preprint (which was not certified by peer review) is the author/funder, who has granted bioRxiv a license to display the preprint in perpetuity. It is made available under aCC-BY 4.0 International license.

358 **Discussion**

359 In the past two decades, the concept that amoeba acts as selective pressure for virulence traits of
360 environmental microbes has gained considerable traction. For fungal pathogens, concordance
361 between virulence factor function in amoeba and macrophages has been demonstrated for *C.*
362 *neoformans* [14,40], *Aspergillus fumigatus* [23,60] and *Paracoccidioides spp.* [24], but many
363 questions remain on how fungal-protozoal interactions select for mammalian virulence. In this
364 study, we investigated how interactions with amoebae affected the phenotype and genotype of *C.*
365 *neoformans* to explore the mechanisms behind this long-term evolutionary adaptation. Our
366 results provide new insights on how amoeba predation can drive the evolution of *C. neoformans*
367 since survivors emerge that show major phenotypic and genetic differences from the founder
368 strain. The phenotypic diversity may facilitate *C. neoformans* adaptation to different hosts and
369 thus enhance its virulence.

370 Pseudohyphae formation was the most common response to *C. neoformans* survival when faced
371 with amoeba predation. This result confirms an older observation that pseudohyphal formation
372 was a 'escape hatch' for *C. neoformans* survival when preyed upon by amoebae [61]. Different
373 fungal morphologies are reported to trigger different killing mechanisms by amoeba [62] and the
374 *C. neoformans* filamentous form may be more resistant to killing. Similar to our observation,
375 Nielson et al [61] reported that when *C. neoformans* was co-cultured with amoebae, most of the
376 fungal cells were killed with survivors forming colonies that contained pseudohyphae. Most of
377 their isolates remained pseudohyphal, with only one out of eight isolates reverting back to the
378 yeast form. That result differed from ours, since most of the pseudohyphal isolates in this study
379 reverted to yeast forms after removal from the amoebae culture, such that only 3 of 18 isolates
380 studied in detail maintained a stable pseudohyphal phenotype. Those three isolates (A4 - A6)

bioRxiv preprint doi: https://doi.org/10.1101/2020.08.07.241190; this version posted August 7, 2020. The copyright holder for this preprint (which was not certified by peer review) is the author/funder, who has granted bioRxiv a license to display the preprint in perpetuity. It is made available under aCC-BY 4.0 International license.

381 have a single nucleotide deletion in *TAO3* gene shown in whole genomic sequencing, and
382 consistent to mutations in RAM/MOR pathway ofthe pseudohyphal variants reported in the
383 previous study [52].

384 Previous studies have focused primarily on cryptococcal isolates with pseudohyphae phenotypes
385 derived from amoeba, but in this study, we investigated in detail those amoeba-resistant isolates
386 with unstable pseudohyphal phenotypes. We found that although some of the isolates (H13. H16,
387 H17) reverted to yeast, they were able to form pseudohyphae quicker than their parental strain
388 when they were exposed to amoebae again. These isolates were less virulent in *Galleria*
389 infection model, a finding consistent with prior reports that the pseudohyphae strains were less
390 virulent in animal models. Interaction with amoebae also resulted in measurable virulence-
391 related phenotypic changes in *C. neoformans*, confirming that amoebae can play a powerful role
392 in the selection of virulence factors, which are related to the pathogenesis of human disease. Of
393 note, we selected only six isolates from each strain for further characterization, but all of them
394 had changes, suggesting that the microevolution occurs frequently and rapidly when exposed to
395 amoebae. Moreover, the changes were pleiotropic and included differences in colony
396 morphology, capsule size, cell size, urease activity, melanin production, susceptibility to thermal
397 stress and an antifungal drug. However, isolates studied revealed a different configuration of
398 phenotypic changes although they tended to cluster in groups from the same survival
399 pseudohyphal colony (S7 Fig). Overall, the interaction of *C. neoformans* with amoebae-
400 passaged isolates with increased phenotype diversity. Since there are many types of amoeboid
401 predators in the soil and *C. neoformans* does not know the identity of the phagocytic predator,
402 generating great diversity in strains could provide this fungus with insurance that some will

bioRxiv preprint doi: https://doi.org/10.1101/2020.08.07.241190; this version posted August 7, 2020. The copyright holder for this preprint (which was not certified by peer review) is the author/funder, who has granted bioRxiv a license to display the preprint in perpetuity. It is made available under aCC-BY 4.0 International license.

403 survive. Hence, the diversity observed among isolates that survived amoeba predation suggests a
404 bet hedging strategy for survival based on the generation of phenotypic diversity.

405 To identify the mechanism for the phenotypic changes, we compared the whole genome
406 sequencing of isolates and ancestral strains using deep sequencing to identify point mutations,
407 amplification or deletion of chromosomal segments and whole-chromosome aneuploidy. We
408 found that there were only two SNPs in H99 derived isolates, four SNPs and two indels in the
409 A1-35-8 derived isolates. Isolates from the same survival pseudohyphal colonies had similar
410 SNPs, which is consistent with the similarity of their phenotypic changes, suggesting that the
411 point mutations may be associated with some of the phenotypic changes. Interestingly, there
412 were total 252 SNPs in Ftc555-1 derived isolates with an average of 48 SNPs among isolates
413 (range of 22-80), a rate approximately10 times higher than H99 and A1-35-8. That may be
414 explained by the fact that the ancestral Ftc555-1 strain contains a splice donor site mutation in
415 *MLH1,* a gene involved in mismatch repair of nuclear DNA. This predicted high impact, loss of
416 function mutation (G to A change at position 1270268 of chr 6) is also found in all sequenced
417 Ftc555-1 progeny isolates. Since the Idnurm laboratory has reported that the loss of *MLH1*
418 results in elevated mutation rates [63], Ftc555-1 is likely to be a hypermutator strain. Increased
419 mutation rates will drive phenotypic variations and some of those may be adaptive for survival in
420 stressful environments, leading to rapid microevolution. On the other hand, the sequencing
421 revealed that one gene (CNAG_03013; *OPT1*) was impacted by non-synonymous SNP changes
422 and single nucleotide deletion in all three strain backgrounds. *OPT1* has been identified by
423 Madhani group as an oligopeptide transporter required for transporting Qsp1, a quorum sensing
424 peptide, into the receiving cells [53]. Deletion of *OPT1* exhibits similar phenotypes to our
425 isolates, including increased capsule size and reduced melanin production, suggesting that this

bioRxiv preprint doi: https://doi.org/10.1101/2020.08.07.241190; this version posted August 7, 2020. The copyright holder for this preprint (which was not certified by peer review) is the author/funder, who has granted bioRxiv a license to display the preprint in perpetuity. It is made available under aCC-BY 4.0 International license.

426 mutation may cause some of the phenotypic changes in our isolates. By reviewing the published
427 sequences of 387 clinical and environments strains [64], we found that 6 of 287 clinical isolates
428 contains high impact, potential loss of function mutations in *OPT1*, but no *OPT1* mutations in
429 those 100 environmental isolates. The Fraser laboratory also reported that one of the clinical
430 isolates in their study contains an inversion in chromosome 3 and affect two genes while one of
431 them are *OPT1* [65]. The relatively high frequency of mutations in *OPT1* among clinical isolates
432 suggests that this gene may be under particular selection during human infection. Another
433 interesting gene mutation found in Ftc555-1 isolates was in the gene *PKR1*. This was a high
434 impact mutation in F3, F4, F5 and F6, which exhibited phenotypes of titan cells and enlarged
435 capsules inside macrophages and in macrophage medium. Pkr1 is known to be a negative
436 regulator of titan cells and capsule enlargements in laboratory strains and clinical isolates
437 [58,66]. A *pkr1* deletion mutant exhibit both enlarged capsule and titan cell production. It is also
438 hypervirulent in a murine infection model [58].
439

440 The relatively low number of SNPs raises the question on how some of these strains change
441 rapidly in response to amoeba predation that result in such broad and rapid phenotypic changes.
442 Therefore, we also investigated the impact of whole-chromosome aneuploidy on isolates. An
443 extra copy of chromosome 8 has been found in three isolates (H13, H16 and H17) which were
444 isolated from the same pseudohyphal survival colony. Aneuploidy is caused by abnormal
445 chromosomal segregation and can happen within even a single mitotic division, so this type of
446 mutant can occur rapidly. This drastic DNA structural change often results in decreased fitness
447 [67]. However, when fungi are exposed to stress, such as antifungal drugs, specific chromosomal
448 aneuploidies can be advantageous through selection for increased gene expression of a subset of

bioRxiv preprint doi: https://doi.org/10.1101/2020.08.07.241190; this version posted August 7, 2020. The copyright holder for this preprint (which was not certified by peer review) is the author/funder, who has granted bioRxiv a license to display the preprint in perpetuity. It is made available under aCC-BY 4.0 International license.

449 genes [55,68–72]. In *C. albicans* and *C. neoformans*, extra copies of specific chromosome
450 containing drug resistance genes have been frequently found in antifungal drug resistance strains
451 [55,70,71]. Likewise, *C. neoformans* could gain an extra chromosome as a solution for
452 adaptation when the fungi encounter threats from amoebae. For instance, chromosome 8 contains
453 one gene (*ZNF2*) which encodes a zinc-finger transcription factor that drives hyphal growth upon
454 overexpression [73]. Chromosome 8 also contains another gene (*CBK1*) that is responsible for
455 pseudohyphal formation [52,74]. *CBK1* encodes serine/threonine protein kinase which is one of
456 the components of RAM pathway. Mutants in the RAM pathway have pseudohyphal phenotype,
457 but we are not aware of any reports showing the effect of the overexpression of *CBK1* on
458 pseudohyphae morphology. Since filamentous morphologies are important for resistance to
459 phagocytosis by amoebae, it is possible that duplication of chromosome 8 could increase the
460 cryptococcal fitness rapidly after exposure to amoebae. Indeed, when we re-introduced those
461 aneuploid strains to amoebae, they could switch to filamentous forms quicker than their ancestor
462 and efficiently resisted killing by amoebae. When we eliminated the chromosomal duplication,
463 the phenotypes were restored back to wildtype level, supporting that there is strong link between
464 duplication of chromosome 8 and amoebae resistance and other changes on virulence phenotypes
465 such as capsule size and urease activity. In addition, there is no point mutations or structural
466 changes such as amplification or deletion of chromosomal segments in these isolates. Therefore,
467 aneuploidy may be the major source of the phenotypic change in that particular group of isolates.
468

469 Pseudohyphae are chains of elongated yeast cells that are unable to undergo cytokinesis
470 completely, leading to multinuclei. Multinucleated cells showed a high level of chromosome
471 instability, resulting in polyploidy and aneuploidy in eukaryotic cells [56]. Previous study of

bioRxiv preprint doi: https://doi.org/10.1101/2020.08.07.241190; this version posted August 7, 2020. The copyright holder for this preprint (which was not certified by peer review) is the author/funder, who has granted bioRxiv a license to display the preprint in perpetuity. It is made available under aCC-BY 4.0 International license.

472 live-cell imaging on *Candida albicans* showed that hyphal cells occasionally generated
473 multinucleated yeast cells [75], with polyploidy and/or aneuploidy, but there are very limited
474 studies on whether pseudohyphal or hyphal formation may directly affect the ploidy variation. In
475 this study, nuclear division, detected with GFP-H2B, was observed in cryptococcal
476 pseudohyphae isolated from amoebae culture. The time-lapse imaging detected a nuclear fusion
477 event, suggesting the cell experienced atypical nuclear division and potentially may undergo
478 polyploidization which frequently generates their offspring with amplification of chromosomal
479 segments or whole-chromosome aneuploidy. This result implies that interaction with amoebae
480 not only contributes to the selection and maintenance of traits in *C. neoformans*, but also may
481 drive heritable variation through pseudohyphae formation.
482

483 The 'amoeboid predator-fungal animal virulence hypothesis' formulates the notion that the
484 capacity for virulence in soil fungi with no need for an animal host arose accidently from the
485 traits for survival against ameboid predators that accidently also functioned as virulence factors
486 for animal infection [12]. Consistent with this notion there is a remarkable concordance between
487 fungal phenotypes that promote survival against amoeba and in animal hosts [14,23] and passage
488 in amoeba is associated with increased virulence for several fungal species [24,39,76]. Analysis
489 of virulence for the amoeba-selected strains described in our study in wax moths revealed no
490 major changes in virulence from the parental strains. It is possible that this host does not
491 discriminate between passaged and non-passaged *C. neoformans* cells or that none of the isolates
492 tested gained or lost traits associated with virulence in that particular host. It is also possible that
493 these strains already had the maximum pathogenic potential [77] for these animal hosts, which
494 could not be further increased by amoeba interactions. However, we did observe that some

bioRxiv preprint doi: https://doi.org/10.1101/2020.08.07.241190; this version posted August 7, 2020. The copyright holder for this preprint (which was not certified by peer review) is the author/funder, who has granted bioRxiv a license to display the preprint in perpetuity. It is made available under aCC-BY 4.0 International license.

495 amoeba-passaged strains were significantly more cytotoxic for macrophages *in vitro*. This result
496 is consistent to the finding that which those strains also had great resistance to amoebae killing.
497 The mechanism behind that is still unclear. However, those particular amoeba-passage strains
498 can form larger cell size and capsule in both amoebae and macrophage culture and that may help
499 them to escape from and cause damages to the host cells. These results fit the theory that
500 amoebae are the training grounds for macrophage resistance of pathogens since the hostile
501 environments in amoebae and macrophage are similar. Among these strains, the virulence of
502 isolates F5 and F6 were further tested in murine infection model. These particular strains were
503 picked because they acquired a mutation in *PKR1*, and deletion of *PKR1* has been shown to
504 increase virulence [58]. However, neither F5 and F6 exhibited hypervirulence phenotype during
505 murine infection, and instead were cleared faster than their parental isolate. It is noteworthy that
506 the nonsense mutation found in F5 and F6 located in codon 407 which is only 75 codons prior to
507 the original stop codon of *PKR1*. It is possible that the mutation results in altered function rather
508 than loss of function and this is not sufficient to reproduce the hypovirulence phenotype caused
509 by full *PKR1* knockout. Microbial virulence is a complex property that is expressed only in a
510 susceptible host and host damage can come from the microbe or the immune response. Both F5
511 and F6 were able to establish themselves in the lung but triggered a more effective immune
512 responses that cleared them. This finding implies the occurrence of other amoeba-selected
513 changes that affect the immune response including overriding of the hypervirulence phenotype
514 caused from the mutation of *PKR1* by compensation from other mutations or changes.

515 The amoeba-passaged *C. neoformans* selected in our study differ from those reported in prior
516 studies [24,39,76] in that they did not increase in virulence. Instead, we observed reductions in
517 murine virulence for two of the isolates studied despite increased capacity to damage

bioRxiv preprint doi: https://doi.org/10.1101/2020.08.07.241190; this version posted August 7, 2020. The copyright holder for this preprint (which was not certified by peer review) is the author/funder, who has granted bioRxiv a license to display the preprint in perpetuity. It is made available under aCC-BY 4.0 International license.

518 macrophages from their long interaction with amoeba. Given the pleiotropic changes observed in
519 our isolate set it is possible that we did not sample sufficient numbers to observed more virulent
520 strains. Our study differs from prior amoeba-*C. neoformans* studies [39] in that it involved
521 prolonged selection on a semi-solid agar surface in conditions that favored the protozoal cells by
522 the presence of cations. In these conditions, amoeba dominance is manifested by a zone of
523 fungal growth clearance where only occasional *C. neoformans* colonies emerged after several
524 weeks. These colonies presumably emerged from resistant cells that survived the initial amoeba
525 onslaught and gave rise to the variant strains that were analyzed in this study. We posit that
526 these amoeba-resistant cells were very rare in the parent *C. neoformans* population and had
527 emerged from the mechanisms discussed above, namely mutation and aneuploidy, which by
528 chance conferred upon those cells amoeba resistance. Alternatively, those colony ancestor cells
529 represent rare cells that were able to sense the amoeba danger and turn on diversity generating
530 mechanisms that occasionally produced amoeba-resistant strains. In this regard, *C. neoformans*
531 can sense amoeba and respond by increasing the size of its capsule by sensing protozoal
532 phospholipids [40] but this process takes time and fungal cell survival probably depends on the
533 race between adaptation and predation. The selection versus adaptation explanations for the
534 origin of these are not mutually exclusive and both could have been operational in these
535 experiments. These survivor cells then grew into a colony under constant amoeba selection
536 where they gave rise to progeny cells where these phenotypic diversity generating mechanisms
537 were maintained and amplified thus accounting for the phenotypic diversity observed in this
538 study.

539

bioRxiv preprint doi: https://doi.org/10.1101/2020.08.07.241190; this version posted August 7, 2020. The copyright holder for this preprint (which was not certified by peer review) is the author/funder, who has granted bioRxiv a license to display the preprint in perpetuity. It is made available under aCC-BY 4.0 International license.

540 In summary, amoebae predation places great selective pressure in *C. neoformans* resulting in the
541 rapid emergence of new phenotypes. The mechanism for these changes includes mutations and
542 aneuploidy, which combine to create great phenotypic diversity. The effect of the phenotype
543 diversification on the fitness of the fungi vary within the same or different hosts, which could
544 promote fungal survival by a bet-hedging strategy that spreads the risk in situations where the
545 environmental threat is unpredictable. Given that human infection also results in rapid fungal
546 microevolution in this host, it is likely that similar mechanisms occur in vivo when this fungus
547 comes under attack by immune cells. Indeed, several studies have shown microevolution of
548 *Cryptococcus* during mammalian infection [65,78–80]. A bet hedging strategy that generates a
549 prodigious number of phenotypes would increase survival in the face of unknown threats and
550 could represent a general mechanism for survival in soils. Interference with the mechanism
551 responsible for generating this plasticity could in turn result in new antimicrobial strategies that
552 would reduce the emergence of diversity and thus simplify the problem for the immune response.
553 Hence, it is interesting to hypothesize that amoeba predation in *C. neoformans* pushes a trigger
554 that sets forth a series of events that generate diversity and similar mechanisms exist in other soil
555 fungi that must routinely confront similar stresses.
556

bioRxiv preprint doi: https://doi.org/10.1101/2020.08.07.241190; this version posted August 7, 2020. The copyright holder for this preprint (which was not certified by peer review) is the author/funder, who has granted bioRxiv a license to display the preprint in perpetuity. It is made available under aCC-BY 4.0 International license.

557 **Method and material**

558 **Ethics statement.** All animal procedures were performed with prior approval from Johns
559 Hopkins University (JHU) Animal Care and Use Committee (IACUC), under approved protocol
560 numbers MO18H152. Mice were handled and euthanized with $CO_2$ in an appropriate chamber
561 followed by thoracotomy as a secondary means of death in accordance with guidelines on
562 Euthanasia of the American Veterinary Medical Association. JHU is accredited by AAALAC
563 International, in compliance with Animal Welfare Act regulations and Public Health Service
564 (PHS) Policy, and has a PHS Approved Animal Welfare Assurance with the NIH Office of
565 Laboratory Animal Welfare. JHU Animal Welfare Assurance Number is D16-00173 (A3272-
566 01). JHU utilizes the United States Government laws and policies for the utilization and care of
567 vertebrate animals used in testing, research and training guidelines for appropriate animal use in
568 a research and teaching setting.

569 **Cell culture.** *Acanthamoeba castellanii* strain 30234 was obtained from the American Type
570 Culture Collection (ATCC). Cultures were clinical isolate of maintained in PYG broth (ATCC
571 medium 712) at 25°C according to instructions from ATCC. *C. neoformans var. grubii* serotype
572 A strain H99 and two environmental isolates A1-35-8 and Ftc555-1 were used for the interaction
573 with amoebae, and these strains were originally obtained from John Perfect (Durham, NC). Both
574 A1-35-8 and Ftc555-1 are environmental strains. A1-35-8 with genotype of VN1 molecular type
575 is isolated from pigeon guano in US while Ftc555-1 is isolated from a mopane tree in Botseana
576 and portrayed VNB molecular type. Both strains were avirulent in mouse model. Histone 2B-
577 GFP tagged (C1746) H99 strain which was used for visualization of nuclear division of
578 pseudohyphae was obtained from Kyung Kwon-Chung (Bethesda, MD) [81]. Cryptococcal cells

bioRxiv preprint doi: https://doi.org/10.1101/2020.08.07.241190; this version posted August 7, 2020. The copyright holder for this preprint (which was not certified by peer review) is the author/funder, who has granted bioRxiv a license to display the preprint in perpetuity. It is made available under aCC-BY 4.0 International license.

579 were cultivated in Sabouraud dextrose broth with shaking (120 rpm) at 30°C overnight (16 h)
580 prior to use in all experiments.

581 Bone-marrow derived macrophages (BMDM) were isolated from the marrow of hind leg bones
582 of 5- to 8-wk-old C57BL-6 female mice (Jackson Laboratories, Bar Harbor, ME). For
583 differentiation, cells were seeded in 100 mm TC-treated cell culture dishes (Corning, Corning,
584 NY) in Dulbecco's Modified Eagle medium (DMEM; Corning) with 20 % L-929 cell-
585 conditioned medium, 10 % FBS (Atlanta Biologicals, Flowery Branch, GA), 2mM Glutamax
586 (Gibco, Gaithersburg MD), 1 % nonessential amino acid (Cellgro, Manassas, VA), 1 % HEPES
587 buffer (Corning), 1 % penicillin-streptomycin (Corning) and 0.1 % 2-mercaptoethanol (Gibco)
588 for 6-7 days at 37 °C with 9.5 % $CO_2$. Fresh media in 3 ml were supplemented on day 3 and the
589 medium were replaced on day 6. Differentiated BMDM were used for experiments within 5 days
590 after completed differentiation.

591 **Assay of *A. castellanii* and *C. neoformans* interaction.** Two hundred *C. neoformans* yeast cells
592 were spread on Sabouraud agar, and incubated at 30 °C overnight. *A. castellanii* in total $5 \times 10^3$
593 cells were dropped randomly at several locations on the agar plate containing *C. neoformans*.
594 Plates were sealed with parafilm and incubated at 25 °C for 3-4 months until survival colonies of
595 *C. neoformans* emerged.

596 To isolate individual cell (hyphae or pseudohyphae in this case) out from the colony (Fig 1D),
597 survival colonies were randomly picked from the plate to a 3 cm culture dish with PBS using
598 pipette tips. Individual cells were picked under a light microscopy using pipette and transferred
599 into a fresh Sabouraud agar. The plates were incubated at 30 °C. After 24 h incubation, the
600 morphologies of microcolony were visualized using a Zeiss Axiovert 200M inverted microscope
601 with a 10× phase objective. After 72 h incubation, colony morphologies were examined using

bioRxiv preprint doi: https://doi.org/10.1101/2020.08.07.241190; this version posted August 7, 2020. The copyright holder for this preprint (which was not certified by peer review) is the author/funder, who has granted bioRxiv a license to display the preprint in perpetuity. It is made available under aCC-BY 4.0 International license.

602 Olympus SZX9 microscope with 1x objective and 32x zoom range. Morphologies of cells from
603 colonies were visualized using Olympus AX70 microscope with 20x objective using the
604 QCapture Suite V2.46 software (QImaging, Surrey, Canada).

605 **Amoebae killing assa**y. *C. neoformans* in 5 × $10^6$ cells were spread as a cross onto Sabouraud
606 agar, and incubated at 30 °C for overnight. *A. castellanii* ($10^4$) cells were dropped at the center of
607 the *C. neoformans* cross. The plates were sealed in parafilm, and incubated at 25 °C. The
608 distance from center to the edge of the clear predator zones in four directions was measured after
609 1-3 weeks incubation. The data were represented as the average of the distances of clear zone
610 from four direction.

611 *C. neoformans* cells were also taken from the edge of the clear zone and at the end of the cross
612 after 1- week incubation, and visualized using Olympus AX70 microscope with 20x objective.
613 For samples of Ftc555-1 strains, the cells were counterstained with India ink.

614 **Capsule and cell size.** *C. neoformans* cells were incubated in minimal medium (15 mM
615 dextrose, 10 mM $MgSO_4$, 29.4 mM $KH_2PO_4$, 13 mM glycine, 3 μM thiamine-HCl) at 30 °C for
616 72 h. In addition, Ftc555-1 and its isolates were incubated in medium for BMDM at 37 °C for 24
617 h. BMDM (1.5 × $10^6$ cells) were also infected with Ftc555-1 and its isolates (1.5 × $10^6$ cells) in
618 6-well plates. After 24 h infection, the culture supernatant was collected and the plates were
619 washed once to collect the extracellular *C. neoformans.* The intracellular *C. neoformans* was
620 collected by lysing the host cell with sterile water.  The cells were stained with 0.1% Uvitex 2B
621 (Polysciences, Warrington, PA) for 10 min and washed two times with PBS. The capsule was
622 visualized by India ink negative staining by mixing cell samples with equal volume of India ink
623 on glass slides and spreading the smear evenly with coverslips. The images with a minimum 100
624 randomly chosen cells was taken by using Olympus AX70 microscopy with 40x objective at

bioRxiv preprint doi: https://doi.org/10.1101/2020.08.07.241190; this version posted August 7, 2020. The copyright holder for this preprint (which was not certified by peer review) is the author/funder, who has granted bioRxiv a license to display the preprint in perpetuity. It is made available under aCC-BY 4.0 International license.

625 bright-field and DAPI channel. The areas of cell body and whole cell (cell body plus capsule)
626 were measured using image J software. The capsule thickness was calculated by subtracting the
627 diameter of whole cell from that of cell body. The cell size was presented as the diameter of cell
628 body without capsule. Three biological independent experiments were performed for each
629 sample.

630 **lactate dehydrogenase (LDH) release assay**. BMDM cells ($5 \times 10^4$ cells/well) were seeded in
631 96-well plates with BMDM for overnight. To initiate the phagocytosis, *C. neoformans* with $5 \times$
632 $10^5$ cells in the presence of 10 μg/ml 18B7 mAb were added in each well of BMDM culture. The
633 culture plates were centrifuged at 1200 rpm for 1 min to settle yeast cells on the monolayer of
634 macrophage culture. After 48 h infection, LDH release were assessed using CytoTox-ONE
635 Homogeneous Membrane Integrity Assay kit (Promega, Madison, WI) according to the
636 manufacturers' instructions.

637 **Urease activity.** *C. neoformans* in $10^8$ cells were incubated in 1 ml of rapid urea broth (RUH)
638 developed by Roberts [82] and adapted by Kwon-Chung [83] at 30 °C. After 1-4 h incubation,
639 cells were collected by centrifugation and 100 μl of supernatant were transferred to 96-well
640 plate. The absorbance of the supernatant was measured at 570 nm using EMax Plus microplate
641 reader (Molecular Devices, San Jose, CA). The assay was performed in Triplicate for each time
642 interval.

643 **Melanin quantification.** *C. neoformans* in $10^4$, $10^5$, $10^6$ and $10^7$ cells were spotted on agar of
644 minimal medium supplemented with 1 mM L-DOPA (Sigma Aldrich, St Louis, MO). The plates
645 were incubated at 30 °C without light. Photos were taken after 1-3-day incubation on a white
646 light illuminator. The photos of samples were always taken together with their ancestors under
647 the same condition in order to avoid different exposure time or light adjusted by the camera. The

bioRxiv preprint doi: https://doi.org/10.1101/2020.08.07.241190; this version posted August 7, 2020. The copyright holder for this preprint (which was not certified by peer review) is the author/funder, who has granted bioRxiv a license to display the preprint in perpetuity. It is made available under aCC-BY 4.0 International license.

648 obtained photos were then converted to greyscale using image J software. The regions of the
649 colonies were selected and the pixels of each selected region were quantified in grayscale. The
650 relative grayscale of the colonies from samples were normalized by the grayscale of the colonies
651 of ancestors. The representation data shown in this paper are at the cell number of $10^6$ cells and
652 at the time point of 24 h. Three biological independent experiments were performed for each
653 sample.

654 **Macrophage killing assay.** BMDM cells ($5 \times 10^4$ cells/well) were infected with *C. neoformans*
655 ( $5 \times 10^4$ cells) in the presence of 10 µg/ml 18B7 mAb. The culture plates were centrifuged at
656 1200 rpm for 1 min to settle yeast cells on the monolayer of macrophage culture. After 24 h
657 infection, phagocytized cryptococcal cells were released by lysing the macrophages with
658 sterilized water. The lysates were serially diluted, plated onto Sabouraud agar and incubated at
659 30 °C for 48 h for colony form unit (CFU) determination. This experiment was performed in
660 triplicates for each strain.

661 **Virulence assay in *Galleria mellonella*.** *G. mellonella* larvae were purchased from Vanderhorst
662 Wholesale (Saint Mary's, OH). Larvae were picked based on weight (175 – 225 mg) and
663 appearance (creamy white in color). Larvae were starved overnight at room temperature. Next
664 day, overnight cultures of *C. neoformans* that grew in Sabouraud broth were washed three times
665 with PBS and diluted to $1 \times 10^5$ cells/ml. Cells in 10 µl were injected into the larva via the second
666 last left proleg paw with 31G needles. Infected larvae were incubated at 30 °C and the number of
667 death larvae were scored daily until all the larvae infected with *C. neoformans* ancestral strains in
668 this study were dead. Control groups of larvae were inoculated with 10 µL of sterile PBS.
669 Experiments were repeated at least two times with experimental groups of 15 larvae at a time.

bioRxiv preprint doi: https://doi.org/10.1101/2020.08.07.241190; this version posted August 7, 2020. The copyright holder for this preprint (which was not certified by peer review) is the author/funder, who has granted bioRxiv a license to display the preprint in perpetuity. It is made available under aCC-BY 4.0 International license.

670 **Whole genome sequencing and variant identification.** Genomic DNA was prepared using
671 cetyltrimethylammonium bromide (CTAB) phenol-chloroform extraction as described
672 previously [84]. Genomic DNA was further purified using a PowerClean DNA cleanup kit
673 (QIAGEN, Hilden, Germany). Libraries were constructed using the Illumina DNA Flex Library
674 kit and were sequenced on an Illumina HiSeq2500 to generate paired 150 base reads. An average
675 of 145X sequence depth (range 69-176X) was generated for each sample. All sequence for this
676 project is available in NCBI under BioProject PRJNA640358.

677 Reads were aligned to the *C. neoformans* H99 assembly [85] using BWA mem v0.7.12 [86].
678 Variants were identified using GATK v3.7 [87]; HaplotypeCaller was invoked in GVCF mode with
679 ploidy = 1, and genotypeGVCFs was used to predict variants in each strain. The workflow used to
680 execute these steps on Terra (terra.bio) is available on Github
681 (https://github.com/broadinstitute/fungal-
682 wdl/tree/master/workflows/fungal_variant_calling_gatk3.wdl). Sites were filtered with
683 variantFiltration using QD < 2.0, FS > 60.0, and MQ < 40.0. Genotypes were filtered if the
684 minimum genotype quality < 50, percent alternate allele < 0.8, or depth < 10
685 (https://github.com/broadinstitute/broad-
686 fungalgroup/blob/master/scripts/SNPs/filterGatkGenotypes.py). Genomic variants were
687 annotated and the functional effect was predicted using SnpEff v4.1g [88].

688 **Cryptococcal cell karyotyping.** Cell karyotypes were analyzed by quantitative PCR. qPCR
689 primers used in this study have been published in Gerstein et al. 2015. qPCR reactions were
690 performed in a StepOnePlus Real-Time PCR System (Applied Biosciences, Beverly Hills, CA)
691 using 20 µl reaction volumes. All reactions were set up in technical triplicate. Each reaction
692 mixture contained PowerUp SYBR Green Master Mix (Applied Bioscience), 300 nM each

bioRxiv preprint doi: https://doi.org/10.1101/2020.08.07.241190; this version posted August 7, 2020. The copyright holder for this preprint (which was not certified by peer review) is the author/funder, who has granted bioRxiv a license to display the preprint in perpetuity. It is made available under aCC-BY 4.0 International license.

693 primer, 10-ng genomic DNA from CTAB extraction, and distilled water (dH2O). Cycling
694 conditions were 95°C for 5 min followed by 40 cycles of 95°C for 15 s and 55°C for 1 min. Melt
695 curve analysis was performed in 0.5°C increments from 55 to 95°C for 5 s for each step to verify
696 that no primer dimers or product from misannealed primers had been amplified. Threshold cycle
697 (CT) values were obtained using StepOnePlus software version 2.3 (Applied Bioscience) where
698 the threshold was adjusted to be within the geometric (exponential) phase of the amplification
699 curve. Chromosome copy numbers were determined using a modified version of the classical CT
700 method as described by [69].

701 **Visualization of nuclear division in pseudohyphae.** Histone 2B-GFP tagged H99 (C1746) was
702 interacted with *A. castellanii* on Sabouraud agar as described above until survival colonies with
703 pseudohyphae emerged. The colonies were transferred on the well of 18B7 Ab coated coverslip
704 bottom MatTek petri dishes with 14mm microwell (MatTek Brand Corporation, Ashland, MA)
705 in minimal medium. After 30 min incubation to allow for settling down the cells, 2 ml of
706 minimal medium were added. Images were taken every 10 min for 24 h using of a Zeiss Axiovert
707 200M inverted microscope with a 10x phase objective and GFP channel in an enclosed chamber
708 under conditions of 30 °C.

709 **Measurement of global histone H3 acetylation.** A culture of *C. neoformans* in 2 ml was grown
710 in Sabouraud broth for 24 h. Protein samples were extracted by vortexing for 4 h with 0.5 mm
711 glass beads and yeastbuster extraction buffer (Merck, Darmstadt, Germany) at 4 °C. Supernatant
712 were collected and 100% trichloroacetic acid was added at a 1:4 ratio. The mixtures were
713 incubated on ice for 30 min, and pellets were then collected by centrifugation at 13,000 g for 10
714 min at 4°C. Pellets were washed twice with 1 ml acetone and dissolved in 20 µl water. The
715 protein concentrations were measured by using Micro BCA™ Protein Assay Kit (Themofisher,

bioRxiv preprint doi: https://doi.org/10.1101/2020.08.07.241190; this version posted August 7, 2020. The copyright holder for this preprint (which was not certified by peer review) is the author/funder, who has granted bioRxiv a license to display the preprint in perpetuity. It is made available under aCC-BY 4.0 International license.

716 Waltham, Ma). The protein samples (3.5 μg) were used to detect the global histone H3
717 acetylation levels by using the EpiQuik global histone H3 acetylation assay kit (EpigenTek,
718 Farmingdale, NY) according to manufacturer's instructions.

719 **Stress sensitivity test.** The overnight cultures were diluted in Sabouraud broth to an $OD_{600}$ of 2
720 and further diluted 10-, $10^2$-, $10^3$-, $10^4$- , $10^5$- fold. The dilutions (5 μl) were spotted onto
721 Sabouraud agar plates supplemented with 16 μg/ml fluconazole and incubated for 48 h at 30 °C.
722 Plates without fluconazole were also incubated for 48 h either 30 or 37 °C.

723 **Growth curve.** *C. neoformans* strains Ftc555-1, F5 and F6 were grown in Sabouraud media at
724 30°C with orbital shaker (120 rpm) for 7 days with data measurements each 24 hours. The assay
725 was performed in a 96-well plate and some serial dilutions were done, with a cell concentration
726 range between 1.0 X $10^7$ to 5.0 x $10^3$/well. Each condition was done in triplicate. The growth was
727 measured by optical density at 600 nm.

728 **Murine Infection.** Six-week-old female A/J mice were infected intranasally with 20 μl of 1.0 X
729 $10^7$ yeast cells of each *C. neoformans* strain. Three groups of mice (n = 8 animals per group) were
730 infected and deaths were scored daily for 60 days. No death was observed during this time, so we
731 decided to euthanize the animal for fungal burden assessment and cytokines levels determination.
732 A second experimental infection was performed with some modifications. Six-week-old female
733 A/J mice were infected intranasally with 20 μl of 1.0 X $10^7$ yeast cells of each *C. neoformans* strain
734 (n = 5 animal per group) and then euthanized after 5 days. Specific organs were removed for fungal
735 burden and cytokines level evaluation.

736 **Fungal burden assessment.** The fungal burden was measured by counting CFU (colony-forming
737 units). After animals euthanasia, the lungs were removed, weighed and homogenized in 1 ml of

bioRxiv preprint doi: https://doi.org/10.1101/2020.08.07.241190; this version posted August 7, 2020. The copyright holder for this preprint (which was not certified by peer review) is the author/funder, who has granted bioRxiv a license to display the preprint in perpetuity. It is made available under aCC-BY 4.0 International license.

738 PBS. After serial dilutions, homogenates were inoculated onto Sabouraud agar plates with 10 U/ml
739 of streptomycin/penicillin. The plates were incubated at room temperature, and the colonies were
740 counted after 48-72 h.

741 **Determination of cytokine levels in the organs.** Spleen and lungs of each mouse were macerated
742 with protease inhibitor (complete, EDTA-free, Roche Life Science, Indiana, United States) and
743 centrifuged; supernatants of these samples were used for cytokine detection by a sandwich-ELISA
744 by using commercial kits (BD OptEIA™, BD Franklin Lakes, Nova Jersey, US) for the following
745 cytokines: IL-2 (#555148), IL- 4 (#555232), IL-10 (#555252), IFN-γ (#551866) and TNF-α
746 (#555268).The protocol was followed according to the manufacturer's recommendations. The
747 reading was performed in a plate spectrophotometer at 450 nm and 570 nm.

748

749

bioRxiv preprint doi: https://doi.org/10.1101/2020.08.07.241190; this version posted August 7, 2020. The copyright holder for this preprint (which was not certified by peer review) is the author/funder, who has granted bioRxiv a license to display the preprint in perpetuity. It is made available under aCC-BY 4.0 International license.

750 **Acknowledgements**

751 We thank the Broad Institute Microbial Omics Core for generating the DNA libraries and the

752 Genomics Platform for the sequence for this study.

753

754

bioRxiv preprint doi: https://doi.org/10.1101/2020.08.07.241190; this version posted August 7, 2020. The copyright holder for this preprint (which was not certified by peer review) is the author/funder, who has granted bioRxiv a license to display the preprint in perpetuity. It is made available under aCC-BY 4.0 International license.

755

756 Table 1. High and moderate impact SNPs found in passaged isolates

| Isolates | Chr | Position | Reference | Alternate | Gene ID | Gene function | Effect of mutation |
|---|---|---|---|---|---|---|---|
| H1, H2, H14 | 3 | 211613 | T | G | CNAG_03013 | Oligopeptide transporter | M484R |
| H1, H2, H14 | 6 | 68953 | C | A | CNAG_02531 | Calcium-dependent protein kinase | Intron variant |
| A1 | 5 | 1208219 | T | C | CNAG_01101 | Hypothetical protein | R478G |
| A2, A3 | 3 | 213165 | G | A | CNAG_03013 | Oligopeptide transporter | Nonsense mutation W932* |
| A2, A3 | 3 | 594765 | A | G | CNAG_02858 | Adenylsuccinate synthetase | I346V |
| A2 | 13 | 592173 | C | T | | Intergenic region | |
| F1† | 3 | 213566 | G | T | CNAG_03013 | Oligopeptide transporter | Splice site mutation |
| F5, F6† | 1 | 1469244 | C | A | CNAG_00570 | cAMP-dependent protein kinase regulator | Nonsense mutation G407* |
| FC2† | 11 | 136455 | T | G | CNAG_01506 | Hypothetical protein | Splice site mutation |

757 † Only high impact mutations of Ftc555-1 variants were shown in this table.

758 Table 2 High impact indels found in passaged A1-35-8 isolates

| Isolates | Chr | Position | Reference | Alternate | Gene ID | Gene function | Effect of mutation |
|---|---|---|---|---|---|---|---|
| A1 | 3 | 211137 | GC | G | CNAG_03013 | Oligopeptide transporter | Frameshift at P358 |
| A4, A5, A6 | 2 | 363200 | CA | C | CNAG_03622 | Cell polarity | Frameshift at N150 |

759

760

bioRxiv preprint doi: https://doi.org/10.1101/2020.08.07.241190; this version posted August 7, 2020. The copyright holder for this preprint (which was not certified by peer review) is the author/funder, who has granted bioRxiv a license to display the preprint in perpetuity. It is made available under aCC-BY 4.0 International license.

761 ## References


762 1. Rajasingham R, Smith RM, Park BJ, Jarvis JN, Govender NP, Chiller TM, et al. Global burden of
763 disease of HIV-associated cryptococcal meningitis: an updated analysis. The Lancet Infectious
764 Diseases. 2017;0. doi:10.1016/S1473-3099(17)30243-8

765 2. Cross CE, Bancroft GJ. Ingestion of acapsular Cryptococcus neoformans occurs via mannose and
766 beta-glucan receptors, resulting in cytokine production and increased phagocytosis of the
767 encapsulated form. Infect Immun. 1995;63: 2604–2611.

768 3. Johnston SA, May RC. Cryptococcus interactions with macrophages: evasion and manipulation of
769 the phagosome by a fungal pathogen. Cell Microbiol. 2013;15: 403–411. doi:10.1111/cmi.12067

770 4. Kozel TR. Non-encapsulated variant of Cryptococcus neoformans. II. Surface receptors for
771 cryptococcal polysaccharide and their role in inhibition of phagocytosis by polysaccharide. Infect
772 Immun. 1977;16: 99–106.

773 5. Vecchiarelli A. Immunoregulation by capsular components of Cryptococcus neoformans. Med
774 Mycol. 2000;38: 407–417.

775 6. Cox GM, Mukherjee J, Cole GT, Casadevall A, Perfect JR. Urease as a Virulence Factor in
776 Experimental Cryptococcosis. Infect Immun. 2000;68: 443–448.

777 7. Cox GM, McDade HC, Chen SCA, Tucker SC, Gottfredsson M, Wright LC, et al. Extracellular
778 phospholipase activity is a virulence factor for Cryptococcus neoformans. Molecular Microbiology.
779 2001;39: 166–175. doi:10.1046/j.1365-2958.2001.02236.x

780 8. Emmons CW. ISOLATION OF CRYPTOCOCCUS NEOFORMANS FROM SOIL. J Bacteriol. 1951;62: 685–
781 690.

782 9. Emmons CW. Saprophytic sources of Cryptococcus neoformans associated with the pigeon
783 (Columba livia). Am J Hyg. 1955;62: 227–232.

784 10. Lazera MS, Salmito Cavalcanti MA, Londero AT, Trilles L, Nishikawa MM, Wanke B. Possible
785 primary ecological niche of Cryptococcus neoformans. Med Mycol. 2000;38: 379–383.

786 11. Castro e Silva DM, Santos DCS, Martins MA, Oliveira L, Szeszs MW, Melhem MSC. First isolation of
787 Cryptococcus neoformans genotype VNI MAT-alpha from wood inside hollow trunks of Hymenaea
788 courbaril. Med Mycol. 2016;54: 97–102. doi:10.1093/mmy/myv066

789 12. Casadevall A, Fu MS, Guimaraes AJ, Albuquerque P. The 'Amoeboid Predator-Fungal Animal
790 Virulence' Hypothesis. Journal of Fungi. 2019;5: 10. doi:10.3390/jof5010010

791 13. Ophir T, Gutnick DL. A Role for Exopolysaccharides in the Protection of Microorganisms from
792 Desiccation. Appl Environ Microbiol. 1994;60: 740–745.

793 14. Steenbergen JN, Shuman HA, Casadevall A. Cryptococcus neoformans interactions with amoebae
794 suggest an explanation for its virulence and intracellular pathogenic strategy in macrophages. Proc
795 Natl Acad Sci U S A. 2001;98: 15245–15250. doi:10.1073/pnas.261418798

bioRxiv preprint doi: https://doi.org/10.1101/2020.08.07.241190; this version posted August 7, 2020. The copyright holder for this preprint (which was not certified by peer review) is the author/funder, who has granted bioRxiv a license to display the preprint in perpetuity. It is made available under aCC-BY 4.0 International license.

796 15. Jacobson ES, Emery HS. Catecholamine uptake, melanization, and oxygen toxicity in Cryptococcus
797 neoformans. Journal of Bacteriology. 1991;173: 401–403. doi:10.1128/jb.173.1.401-403.1991

798 16. Wang Y, Aisen P, Casadevall A. Cryptococcus neoformans melanin and virulence: mechanism of
799 action. Infection and Immunity. 1995;63: 3131–3136.

800 17. Rosas ÁL, Casadevall A. Melanization affects susceptibility of Cryptococcus neoformans to heat and
801 cold. FEMS Microbiol Lett. 1997;153: 265–272. doi:10.1111/j.1574-6968.1997.tb12584.x

802 18. Wang Y, Casadevall A. Decreased susceptibility of melanized Cryptococcus neoformans to UV light.
803 Appl Environ Microbiol. 1994;60: 3864–3866.

804 19. Fu MS, Coelho C, Leon-Rodriguez CMD, Rossi DCP, Camacho E, Jung EH, et al. Cryptococcus
805 neoformans urease affects the outcome of intracellular pathogenesis by modulating
806 phagolysosomal pH. PLOS Pathogens. 2018;14: e1007144. doi:10.1371/journal.ppat.1007144

807 20. Casadevall A, Perfect JR. Cryptococcus neoformans. American Society of Microbiology; 1998.
808 doi:10.1128/9781555818241

809 21. Cirillo JD, Falkow S, Tompkins LS. Growth of Legionella pneumophila in Acanthamoeba castellanii
810 enhances invasion. Infection and Immunity. 1994;62: 3254–3261.

811 22. Cirillo JD, Falkow S, Tompkins LS, Bermudez LE. Interaction of Mycobacterium avium with
812 environmental amoebae enhances virulence. Infection and Immunity. 1997;65: 3759–3767.

813 23. Novohradská S, Ferling I, Hillmann F. Exploring Virulence Determinants of Filamentous Fungal
814 Pathogens through Interactions with Soil Amoebae. Front Cell Infect Microbiol. 2017;7.
815 doi:10.3389/fcimb.2017.00497

816 24. Albuquerque P, Nicola AM, Magnabosco DAG, Derengowski L da S, Crisóstomo LS, Xavier LCG, et al.
817 A hidden battle in the dirt: Soil amoebae interactions with Paracoccidioides spp. PLOS Neglected
818 Tropical Diseases. 2019;13: e0007742. doi:10.1371/journal.pntd.0007742

819 25. Davies B, Chattings LS, Edwards SW. Superoxide generation during phagocytosis by Acanthamoeba
820 castellanii: similarities to the respiratory burst of immune phagocytes. Microbiology,. 1991;137:
821 705–710. doi:10.1099/00221287-137-3-705

822 26. Davies B, Edwards SW. Chemiluminescence and superoxide production in Acanthamoeba
823 castellanii: free radicals generated during oxidative stress. Microbiology,. 1991;137: 1021–1027.
824 doi:10.1099/00221287-137-5-1021

825 27. Allen PG, Dawidowicz EA. Phagocytosis in Acanthamoeba: I. A mannose receptor is responsible for
826 the binding and phagocytosis of yeast. Journal of Cellular Physiology. 1990;145: 508–513.
827 doi:10.1002/jcp.1041450317

828 28. Allen PG, Dawidowicz EA. Phagocytosis in Acanthamoeba: II. Soluble and insoluble mannose-rich
829 ligands stimulate phosphoinositide metabolism. Journal of Cellular Physiology. 1990;145: 514–521.
830 doi:10.1002/jcp.1041450318

bioRxiv preprint doi: https://doi.org/10.1101/2020.08.07.241190; this version posted August 7, 2020. The copyright holder for this preprint (which was not certified by peer review) is the author/funder, who has granted bioRxiv a license to display the preprint in perpetuity. It is made available under aCC-BY 4.0 International license.

831 29. Brown RC, Bass H, Coombs JP. Carbohydrate binding proteins involved in phagocytosis by
832 Acanthamoeba. Nature. 1975;254: 434–435. doi:10.1038/254434a0

833 30. Lock R, Öhman L, Dahlgren C. Phagocytic recognition mechanisms in human granulocytes and
834 Acanthamoeba castellanii using type 1 fimbriated Escherichia coli as phagocytic prey. FEMS
835 Microbiol Lett. 1987;44: 135–140. doi:10.1111/j.1574-6968.1987.tb02257.x

836 31. Gotthardt D, Warnatz HJ, Henschel O, Brückert F, Schleicher M, Soldati T. High-Resolution
837 Dissection of Phagosome Maturation Reveals Distinct Membrane Trafficking Phases. MBoC.
838 2002;13: 3508–3520. doi:10.1091/mbc.e02-04-0206

839 32. Kwaik YA. The phagosome containing Legionella pneumophila within the protozoan Hartmannella
840 vermiformis is surrounded by the rough endoplasmic reticulum. Appl Environ Microbiol. 1996;62:
841 2022–2028.

842 33. Bozue JA, Johnson W. Interaction of Legionella pneumophila with Acanthamoeba castellanii:
843 Uptake by Coiling Phagocytosis and Inhibition of Phagosome-Lysosome Fusion. INFECT IMMUN.
844 1996;64: 6.

845 34. Horwitz MA. The Legionnaires' disease bacterium (Legionella pneumophila) inhibits phagosome-
846 lysosome fusion in human monocytes. Journal of Experimental Medicine. 1983;158: 2108–2126.
847 doi:10.1084/jem.158.6.2108

848 35. Horwitz MA, Silverstein SC. Legionnaires' Disease Bacterium (*Legionella pneumophila*) Multiplies
849 Intracellularly in Human Monocytes. J Clin Invest. 1980;66: 441–450. doi:10.1172/JCI109874

850 36. Rowbotham TJ. Preliminary report on the pathogenicity of Legionella pneumophila for freshwater
851 and soil amoebae. Journal of Clinical Pathology. 1980;33: 1179–1183. doi:10.1136/jcp.33.12.1179

852 37. Swanson MS, Isberg RR. Association of Legionella pneumophila with the macrophage endoplasmic
853 reticulum. Infect Immun. 1995;63: 3609–3620.

854 38. Arico-Muendel C, Centrella PA, Contonio BD, Morgan BA, O'Donovan G, Paradise CL, et al.
855 Antiparasitic activities of novel, orally available fumagillin analogs. Bioorganic & Medicinal
856 Chemistry Letters. 2009;19: 5128–5131. doi:10.1016/j.bmcl.2009.07.029

857 39. Steenbergen JN, Nosanchuk JD, Malliaris SD, Casadevall A. Cryptococcus neoformans Virulence Is
858 Enhanced after Growth in the Genetically Malleable Host Dictyostelium discoideum. Infection and
859 Immunity. 2003;71: 4862–4872. doi:10.1128/IAI.71.9.4862-4872.2003

860 40. Chrisman CJ, Albuquerque P, Guimaraes AJ, Nieves E, Casadevall A. Phospholipids Trigger
861 Cryptococcus neoformans Capsular Enlargement during Interactions with Amoebae and
862 Macrophages. PLOS Pathogens. 2011;7: e1002047. doi:10.1371/journal.ppat.1002047

863 41. Castellani A. An amoeba growing in cultures of a yeast I II III IV. In: Jour Trop Med & Hyg [Internet].
864 19 Sep 1930 [cited 5 Nov 2019]. Available:
865 https://eurekamag.com/research/030/004/030004150.php

bioRxiv preprint doi: https://doi.org/10.1101/2020.08.07.241190; this version posted August 7, 2020. The copyright holder for this preprint (which was not certified by peer review) is the author/funder, who has granted bioRxiv a license to display the preprint in perpetuity. It is made available under aCC-BY 4.0 International license.

866 42. Castellani A. [Phagocytic and destructive action of Hartmanella castellanii (Amoeba castellanii) on
867 pathogenic encapsulated yeast-like fungi Torulopsis neoformans (Cryptococcus neoformans)]. Ann
868 Inst Pasteur (Paris). 1955;89: 1–7.

869 43. Ruiz A, Neilson JB, Bulmer GS. Control of Cryptococcus neoformans in nature by biotic factors.
870 Sabouraudia. 1982;20: 21–29.

871 44. Garcia-Solache MA, Izquierdo-Garcia D, Smith C, Bergman A, Casadevall A. Fungal virulence in a
872 lepidopteran model is an emergent property with deterministic features. mBio. 2013;4: e00100-
873 00113. doi:10.1128/mBio.00100-13

874 45. Fu MS, Casadevall A. Divalent Metal Cations Potentiate the Predatory Capacity of Amoeba for
875 Cryptococcus neoformans. Appl Environ Microbiol. 2018;84. doi:10.1128/AEM.01717-17

876 46. Chrisman CJ, Alvarez M, Casadevall A. Phagocytosis of Cryptococcus neoformans by, and Nonlytic
877 Exocytosis from, Acanthamoeba castellanii. Appl Environ Microbiol. 2010;76: 6056–6062.
878 doi:10.1128/AEM.00812-10

879 47. Watkins RA, Andrews A, Wynn C, Barisch C, King JS, Johnston SA. Cryptococcus neoformans Escape
880 From Dictyostelium Amoeba by Both WASH-Mediated Constitutive Exocytosis and Vomocytosis.
881 Front Cell Infect Microbiol. 2018;8. doi:10.3389/fcimb.2018.00108

882 48. Derengowski L da S, Paes HC, Albuquerque P, Tavares AHFP, Fernandes L, Silva-Pereira I, et al. The
883 Transcriptional Response of Cryptococcus neoformans to Ingestion by Acanthamoeba castellanii
884 and Macrophages Provides Insights into the Evolutionary Adaptation to the Mammalian Host.
885 Eukaryotic Cell. 2013;12: 761–774. doi:10.1128/EC.00073-13

886 49. Okagaki LH, Strain AK, Nielsen JN, Charlier C, Baltes NJ, Chrétien F, et al. Cryptococcal Cell
887 Morphology Affects Host Cell Interactions and Pathogenicity. PLOS Pathogens. 2010;6: e1000953.
888 doi:10.1371/journal.ppat.1000953

889 50. Zaragoza O, García-Rodas R, Nosanchuk JD, Cuenca-Estrella M, Rodríguez-Tudela JL, Casadevall A.
890 Fungal Cell Gigantism during Mammalian Infection. PLOS Pathogens. 2010;6: e1000945.
891 doi:10.1371/journal.ppat.1000945

892 51. Okagaki LH, Nielsen K. Titan Cells Confer Protection from Phagocytosis in Cryptococcus
893 neoformans Infections. Eukaryot Cell. 2012;11: 820–826. doi:10.1128/EC.00121-12

894 52. Magditch DA, Liu T-B, Xue C, Idnurm A. DNA Mutations Mediate Microevolution between Host-
895 Adapted Forms of the Pathogenic Fungus Cryptococcus neoformans. PLOS Pathogens. 2012;8:
896 e1002936. doi:10.1371/journal.ppat.1002936

897 53. Homer CM, Summers DK, Goranov AI, Clarke SC, Wiesner DL, Diedrich JK, et al. Intracellular Action
898 of a Secreted Peptide Required for Fungal Virulence. Cell Host & Microbe. 2016;19: 849–864.
899 doi:10.1016/j.chom.2016.05.001

900 54. Gerstein AC, Fu MS, Mukaremera L, Li Z, Ormerod KL, Fraser JA, et al. Polyploid Titan Cells Produce
901 Haploid and Aneuploid Progeny To Promote Stress Adaptation. mBio. 2015;6.
902 doi:10.1128/mBio.01340-15

bioRxiv preprint doi: https://doi.org/10.1101/2020.08.07.241190; this version posted August 7, 2020. The copyright holder for this preprint (which was not certified by peer review) is the author/funder, who has granted bioRxiv a license to display the preprint in perpetuity. It is made available under aCC-BY 4.0 International license.

903 55. Sionov E, Lee H, Chang YC, Kwon-Chung KJ. Cryptococcus neoformans Overcomes Stress of Azole
904 Drugs by Formation of Disomy in Specific Multiple Chromosomes. PLOS Pathogens. 2010;6:
905 e1000848. doi:10.1371/journal.ppat.1000848

906 56. Anderson CA, Roberts S, Zhang H, Kelly CM, Kendall A, Lee C, et al. Ploidy variation in multinucleate
907 cells changes under stress. MBoC. 2015;26: 1129–1140. doi:10.1091/mbc.E14-09-1375

908 57. O'Meara TR, Hay C, Price MS, Giles S, Alspaugh JA. Cryptococcus neoformans Histone
909 Acetyltransferase Gcn5 Regulates Fungal Adaptation to the Host. Eukaryot Cell. 2010;9: 1193–
910 1202. doi:10.1128/EC.00098-10

911 58. D'Souza CA, Alspaugh JA, Yue C, Harashima T, Cox GM, Perfect JR, et al. Cyclic AMP-Dependent
912 Protein Kinase Controls Virulence of the Fungal Pathogen Cryptococcus neoformans. Molecular
913 and Cellular Biology. 2001;21: 3179–3191. doi:10.1128/MCB.21.9.3179-3191.2001

914 59. Beenhouwer DO, Shapiro S, Feldmesser M, Casadevall A, Scharff MD. Both Th1 and Th2 Cytokines
915 Affect the Ability of Monoclonal Antibodies To Protect Mice against Cryptococcus neoformans.
916 Kozel TR, editor. Infect Immun. 2001;69: 6445–6455. doi:10.1128/IAI.69.10.6445-6455.2001

917 60. Van Waeyenberghe L, Baré J, Pasmans F, Claeys M, Bert W, Haesebrouck F, et al. Interaction of
918 Aspergillus fumigatus conidia with Acanthamoeba castellanii parallels macrophage-fungus
919 interactions. Environ Microbiol Rep. 2013;5: 819–824. doi:10.1111/1758-2229.12082

920 61. Neilson JB, Ivey MH, Bulmer GS. Cryptococcus neoformans: pseudohyphal forms surviving culture
921 with Acanthamoeba polyphaga. Infect Immun. 1978;20: 262–266.

922 62. Radosa S, Ferling I, Sprague JL, Westermann M, Hillmann F. The different morphologies of yeast
923 and filamentous fungi trigger distinct killing and feeding mechanisms in a fungivorous amoeba.
924 Environ Microbiol. 2019;21: 1809–1820. doi:10.1111/1462-2920.14588

925 63. Billmyre RB, Clancey SA, Heitman J. Natural mismatch repair mutations mediate phenotypic
926 diversity and drug resistance in Cryptococcus deuterogattii. eLife. 6. doi:10.7554/eLife.28802

927 64. Desjardins CA, Giamberardino C, Sykes SM, Yu C-H, Tenor JL, Chen Y, et al. Population genomics
928 and the evolution of virulence in the fungal pathogen Cryptococcus neoformans. Genome Res.
929 2017;27: 1207–1219. doi:10.1101/gr.218727.116

930 65. Ormerod KL, Morrow CA, Chow EWL, Lee IR, Arras SDM, Schirra HJ, et al. Comparative Genomics of
931 Serial Isolates of Cryptococcus neoformans Reveals Gene Associated With Carbon Utilization and
932 Virulence. G3: Genes, Genomes, Genetics. 2013;3: 675–686. doi:10.1534/g3.113.005660

933 66. Hommel B, Mukaremera L, Cordero RJB, Coelho C, Desjardins CA, Sturny-Leclère A, et al. Titan cells
934 formation in Cryptococcus neoformans is finely tuned by environmental conditions and modulated
935 by positive and negative genetic regulators. PLOS Pathogens. 2018;14: e1006982.
936 doi:10.1371/journal.ppat.1006982

937 67. Torres EM, Sokolsky T, Tucker CM, Chan LY, Boselli M, Dunham MJ, et al. Effects of aneuploidy on
938 cellular physiology and cell division in haploid yeast. Science. 2007;317: 916–924.
939 doi:10.1126/science.1142210

bioRxiv preprint doi: https://doi.org/10.1101/2020.08.07.241190; this version posted August 7, 2020. The copyright holder for this preprint (which was not certified by peer review) is the author/funder, who has granted bioRxiv a license to display the preprint in perpetuity. It is made available under aCC-BY 4.0 International license.

940 68. Rancati G, Pavelka N, Fleharty B, Noll A, Trimble R, Walton K, et al. Aneuploidy Underlies Rapid
941 Adaptive Evolution of Yeast Cells Deprived of a Conserved Cytokinesis Motor. Cell. 2008;135: 879–
942 893. doi:10.1016/j.cell.2008.09.039

943 69. Pavelka N, Rancati G, Zhu J, Bradford WD, Saraf A, Florens L, et al. Aneuploidy confers quantitative
944 proteome changes and phenotypic variation in budding yeast. Nature. 2010;468: 321–325.
945 doi:10.1038/nature09529

946 70. Selmecki A, Forche A, Berman J. Aneuploidy and Isochromosome Formation in Drug-Resistant
947 Candida albicans. Science. 2006;313: 367–370. doi:10.1126/science.1128242

948 71. Selmecki A, Gerami-Nejad M, Paulson C, Forche A, Berman J. An isochromosome confers drug
949 resistance in vivo by amplification of two genes, ERG11 and TAC1. Molecular Microbiology.
950 2008;68: 624–641. doi:10.1111/j.1365-2958.2008.06176.x

951 72. Sunshine AB, Payen C, Ong GT, Liachko I, Tan KM, Dunham MJ. The Fitness Consequences of
952 Aneuploidy Are Driven by Condition-Dependent Gene Effects. PLOS Biology. 2015;13: e1002155.
953 doi:10.1371/journal.pbio.1002155

954 73. Lin J, Idnurm A, Lin X. Morphology and its underlying genetic regulation impact the interaction
955 between Cryptococcus neoformans and its hosts. Med Mycol. 2015;53: 493–504.
956 doi:10.1093/mmy/myv012

957 74. Walton FJ, Heitman J, Idnurm A. Conserved Elements of the RAM Signaling Pathway Establish Cell
958 Polarity in the Basidiomycete Cryptococcus neoformans in a Divergent Fashion from Other Fungi.
959 MBoC. 2006;17: 3768–3780. doi:10.1091/mbc.e06-02-0125

960 75. Thomson DD, Berman J, Brand AC. High frame-rate resolution of cell division during Candida
961 albicans filamentation. Fungal Genet Biol. 2016;88: 54–58. doi:10.1016/j.fgb.2016.02.001

962 76. Gonçalves D de S, Ferreira M da S, Gomes KX, Noval CRL, Liedke SC, Costa GCV da, et al.
963 Unravelling the interactions of the environmental host Acanthamoeba castellanii with fungi
964 through the recognition by mannose-binding proteins. Cellular Microbiology. 2019;21: e13066.
965 doi:10.1111/cmi.13066

966 77. Casadevall A. The Pathogenic Potential of a Microbe. mSphere. 2017;2.
967 doi:10.1128/mSphere.00015-17

968 78. Chen Y, Farrer RA, Giamberardino C, Sakthikumar S, Jones A, Yang T, et al. Microevolution of Serial
969 Clinical Isolates of Cryptococcus neoformans var. grubii and C. gattii. mBio. 2017;8.
970 doi:10.1128/mBio.00166-17

971 79. Blasi E, Brozzetti A, Francisci D, Neglia R, Cardinali G, Bistoni F, et al. Evidence of Microevolution in
972 a Clinical Case of Recurrent Cryptococcus neoformans Meningoencephalitis. Eur J Clin Microbiol
973 Infect Dis. 2001;20: 535–543. doi:10.1007/s100960100549

974 80. Sullivan D, Haynes K, Moran G, Shanley D, Coleman D. Persistence, replacement, and
975 microevolution of Cryptococcus neoformans strains in recurrent meningitis in AIDS patients.
976 Journal of Clinical Microbiology. 1996;34: 1739–1744.

bioRxiv preprint doi: https://doi.org/10.1101/2020.08.07.241190; this version posted August 7, 2020. The copyright holder for this preprint (which was not certified by peer review) is the author/funder, who has granted bioRxiv a license to display the preprint in perpetuity. It is made available under aCC-BY 4.0 International license.

977 81. Chang YC, Lamichhane AK, Kwon-Chung KJ. Cryptococcus neoformans, Unlike Candida albicans,
978 Forms Aneuploid Clones Directly from Uninucleated Cells under Fluconazole Stress. mBio. 2018;9.
979 doi:10.1128/mBio.01290-18

980 82. Roberts GD, Horstmeier CD, Land GA, Foxworth JH. Rapid urea broth test for yeasts. J Clin
981 Microbiol. 1978;7: 584–588.

982 83. Kwon-Chung KJ, Wickes BL, Booth JL, Vishniac HS, Bennett JE. Urease inhibition by EDTA in the two
983 varieties of Cryptococcus neoformans. Infect Immun. 1987;55: 1751–1754.

984 84. Velegraki A, Kambouris M, Kostourou A, Chalevelakis G, Legakis NJ. Rapid extraction of fungal DNA
985 from clinical samples for PCR amplification. Medical Mycology. 1999; 5.

986 85. Janbon G, Ormerod KL, Paulet D, Byrnes EJ, Yadav V, Chatterjee G, et al. Analysis of the genome
987 and transcriptome of *Cryptococcus neoformans* var. *grubii* reveals complex RNA expression and
988 microevolution leading to virulence attenuation. PLoS Genet. 2014;10: e1004261.
989 doi:10.1371/journal.pgen.1004261

990 86. Li H. Aligning sequence reads, clone sequences and assembly contigs with BWA-MEM.
991 arXiv:13033997 [q-bio]. 2013 [cited 22 May 2015]. Available: http://arxiv.org/abs/1303.3997

992 87. McKenna A, Hanna M, Banks E, Sivachenko A, Cibulskis K, Kernytsky A, et al. The Genome Analysis
993 Toolkit: a MapReduce framework for analyzing next-generation DNA sequencing data. Genome
994 Res. 2010;20: 1297–303. doi:10.1101/gr.107524.110

995 88. Cingolani P, Platts A, Wang LL, Coon M, Nguyen T, Wang L, et al. A program for annotating and
996 predicting the effects of single nucleotide polymorphisms, SnpEff. Fly (Austin). 2012;6: 80–92.
997 doi:10.4161/fly.19695

998

bioRxiv preprint doi: https://doi.org/10.1101/2020.08.07.241190; this version posted August 7, 2020. The copyright holder for this preprint (which was not certified by peer review) is the author/funder, who has granted bioRxiv a license to display the preprint in perpetuity. It is made available under aCC-BY 4.0 International license.

999 **Figure legends**

1000 Fig 1. *C. neoformans* colonies exhibit various cellular and colony morphologies after co-
1001 incubated with amoebae in Sabouraud agar. (A) Small colonies of H99 (red arrow) surviving in a
1002 mat of amoeba that appears a hazy cloudy area (denoted by dashed line). Typical *C. neoformans*
1003 colonies (CN) are visible on the right bottom of the image. (B) Cells in the survival colony
1004 exhibit hyphal or pseudohyphal morphology (100× magnification). (C) Both pseudohyphae and
1005 yeast cells were identified on a wet mount of samples taken from the survival colony (400x). (D)
1006 Schematic representation of individual hyphae isolation. i. Survival colonies were picked using
1007 pipette tips and transferred to PBS in 3 mm culture dish. ii. Total 20 individual hyphae from 2-4
1008 colonies were selected under microscope and transferred to fresh Sabouraud agar. Plates were
1009 incubated at 30 °C to generate colonies. iii. Six colonies were then selected for further
1010 phenotypic characterization. iv. Control colonies were also picked from the same plate of hyphal
1011 isolates but without interacting with amoeba. (E) Single pseudohyphal cell has been isolated
1012 from the survival colonies and transferred onto a fresh amoebae-free solid medium where form
1013 new colonies. (F) Microcolony with mostly yeast cells has been formed from a single
1014 pseudohyphal cell in 24 h. (G) Colony developed a serrated appearance after 2 days. (H) Yeast
1015 cells were identified on a wet mount of samples taken from the serrated colony. (I-L) Images
1016 showed another example of single pseudohyphal cell isolation. Smooth colony was formed from
1017 this particular pseudohyphal cell. (M-N) Same experiment was performed on environmental
1018 strains A1-35-8 and Ftc-555-1. Various cellular and colony morphologies have been identified
1019 among isolates A1-A6 and F1-F6 in the background of A1-35-8 and Ftc555-1 respectively.
1020 Colonies grew up from individual hyphae which was isolated from the same survival colony
1021 were grouped in red boxes.

bioRxiv preprint doi: https://doi.org/10.1101/2020.08.07.241190; this version posted August 7, 2020. The copyright holder for this preprint (which was not certified by peer review) is the author/funder, who has granted bioRxiv a license to display the preprint in perpetuity. It is made available under aCC-BY 4.0 International license.

1022 Fig 2. Isolates in H99 background derived from exposure to amoeba demonstrated increased
1023 resistance to amoebal killing by rapid pseudohyphal formation. (A) Scheme of amoebae killing
1024 assay. *C. neoformans* was streaked in a cross while *A. castellanii* was dropped at the intersection
1025 of the cross on Sabouraud agar. The data shown are the average of the distance between
1026 boundary and center of clear predator zone in four indicated directions (a-b), with the area being
1027 the predation zone. (B) All of the isolates that had prior exposure to amoeba had smaller clear
1028 zone than their ancestor and controls, consistent with enhanced resistance. A, ancestor; C1-3,
1029 controls; H, isolates derived from H99 after exposure to amoeba. Data are means from three
1030 biological replicates and error bars are SD. (C) Samples were taken from the peripheral areas of
1031 the predator zone after one-week co-incubation with amoebae and visualized under microscope.
1032 All of the isolates showed pseudohyphal formation, but ancestor and controls did not. (D)
1033 Sample were taken from the end of the cross where *C. neoformans* have not contacted with *A.*
1034 *castellanii* yet. All of the isolates manifested yeast cell morphology.

1035 Fig 3. Some of the isolated recovered from the environmental strains A1-35-8 and Ftc-555-1
1036 exhibited increased resistance to *A. castellanii*. (A) No clear predator zone of clearance was
1037 apparent with isolates A4-A6, while larger predator zones were apparent for isolates A1-A3
1038 when comparing to their ancestor. A, ancestor; C1-3, controls; A1-6, isolates derived from A1-
1039 35-8 after exposure to amoeba (B) Isolates F3- F5 showed smaller predator zone than their
1040 ancestor. Data are means from three biological replicates and error bars are SD. A, ancestor; C1-
1041 3, controls; F1-6, isolates derived from Ftc555-1 after exposure to amoeba (C) Ftc-555-1
1042 samples were collected from predator zone after one-week co-incubation. Isolates F3-F6 formed
1043 larger cell size than their ancestor and controls. (D) The cell size of isolates F3-F6 from the end

bioRxiv preprint doi: https://doi.org/10.1101/2020.08.07.241190; this version posted August 7, 2020. The copyright holder for this preprint (which was not certified by peer review) is the author/funder, who has granted bioRxiv a license to display the preprint in perpetuity. It is made available under aCC-BY 4.0 International license.

1044 of the cross is slightly larger than the one of ancestor and controls, but they are not as large as the
1045 cells taken from predator zone.

1046 Fig 4. Capsule thickness for cells of parent strain and amoeba-selected strains. (A) H99 isolates
1047 (B) A1-35-8 isolates and (C) Ftc555-1 isolates have been cultured in minimal medium at 30 °C
1048 for three days. Capsule was visualized by counterstaining with India ink. A, ancestor; C1-3,
1049 controls. * $P < 0.1$ ** $P < 0.01$ **** $P < 0.0001$ by One-way ANOVA, followed by Tukey's
1050 multiple-comparison test.

1051 Fig 5. Cellular dimensions for cells of parent strain and amoeba-selected strains. (A) H99 isolates
1052 (B) A1-35-8 isolates and (C) Ftc555-1 isolates have been cultured in minimal medium for three
1053 days. A, ancestor; C1-3, controls. (D-E) Ftc555-1 isolates have also been cultured in macrophage
1054 medium and with BMDM at 37 °C 9.5% $CO_2$ for 24 h. Extracellular cryptococcal cells were
1055 collected from the culture supernatant while intracellular cells were retrieved from lysing the
1056 BMDM. A, ancestor; C1-3, controls. **** $P < 0.0001$ by One-way ANOVA, followed by
1057 Tukey's multiple-comparison test.

1058 Fig 6. Urease activity for cells of parent strain and amoeba-selected strains. The urease activity
1059 of cryptococcal cells were detected by using rapid urea broth (RUH) method. Amoeba-passaged
1060 isolates with numbers preceded by the letters H, A, and F to indicate their origin from strains
1061 H99, A1-35-8 and Ftc555-1, respectively. A, ancestor; C1-3, controls. The assay was performed
1062 in triplicate for each time point. Error bars represent SD. * $P < 0.1$ ** $P < 0.01$ *** $P < 0.001$ by
1063 unpaired t-test.

1064 Fig 7. Melanization formation for cells of parent strain and amoeba-selected strains.
1065 Melanization was analyzed by spotting the $10^6$ cryptococcal cells on minimal medium agar with

bioRxiv preprint doi: https://doi.org/10.1101/2020.08.07.241190; this version posted August 7, 2020. The copyright holder for this preprint (which was not certified by peer review) is the author/funder, who has granted bioRxiv a license to display the preprint in perpetuity. It is made available under aCC-BY 4.0 International license.

1066 L-DOPA for 24 h. The pigmentation of colony was measured through grayscale pixel
1067 quantification by the software ImageJ. Relative blackness was calculated as a ratio of grayscale
1068 quantification between isolates, their ancestor (A) and control (C1-3). Error bars represent SD. *
1069 $P < 0.1$ ** $P < 0.01$ **** $P < 0.0001$ by unpaired t-test.

1070 Fig 8. The growth of parents and isolates under stress conditions. Cells were 10-fold serially
1071 diluted and spotted onto YPD medium with or without fluconazole (16 µg/ml), and grown for
1072 two days at 30°C or 40°C. Amoeba-passaged isolates with numbers preceded by the letters H, A,
1073 and F to indicate their origin from strains H99, A1-35-8 and Ftc555-1, respectively. A, ancestor;
1074 C1-3, controls.

1075 Fig 9. Aneuploidy plays a role in pseudohyphal formation. (A) Chromosomal copy numbers of
1076 H99 isolates were determined based on depth of sequence coverage normalized by the average
1077 genome-wide sequence depth (B) Relative chromosome copy number of isolate H17 was
1078 obtained by qPCR. H17 have duplication of chromosome 8 (C) chromosome duplication in H17
1079 is eliminated by passaging H17 in fresh Sabouraud medium for 30 days. (D) H17 euploid
1080 ($H17^{Eu}$) strain did not form pseudohyphae as rapid as H17 aneuploid strain. (E) $H17^{Eu}$ euploid
1081 strain has larger predator zone than $H17^{Aneu}$. Data represent the mean of three biological
1082 replicates per biological sample and error bars are SD. (F) $H17^{Eu}$ strain has lower urease activity
1083 then $H17^{Aneu}$ and comparable urease activity as H99 at early time point (1 h) Data represent the
1084 mean of two biological replicates per biological sample and error bars are SD. (G) $H17^{Eu}$ has
1085 smaller capsule size than $H17^{Aneu}$ , but similar capsule size with H99.

1086 Fig 10. Time-lapse imaging showing nuclear division of pseudohyphae. The images of
1087 pseudohyphae of amoeba-passaged H99 GFP-H2B strain were taken by phase-contrast and
1088 fluorescence microscopy. Bud (red arrow) were forming between 0-220 min. The nucleus

bioRxiv preprint doi: https://doi.org/10.1101/2020.08.07.241190; this version posted August 7, 2020. The copyright holder for this preprint (which was not certified by peer review) is the author/funder, who has granted bioRxiv a license to display the preprint in perpetuity. It is made available under aCC-BY 4.0 International license.

1089 migrates into the daughter cells at 240 min, and separated at 300 min. Nuclear division was
1090 completed at 400 min. However, the nucleus from mother cells re-entered into the daughter cells
1091 at 500 min and underwent fusion at 580 min.

1092 Fig 11. (A-C) The survival of parents and isolates in culture with BMDM. The survival of (A)
1093 H99, (B) A1-35-8 and (C) Ftc555-1 isolates was determined by colony form unit (CFU) after 0
1094 and 24 h phagocytosis. The percentage of survival was calculated by normalizing the CFU value
1095 of 24 h infection to time zero. A, ancestor; C1-3, controls. Data represent the mean of three
1096 biological replicates and error bars are SD. (D) BMDM were infected with Ftc555-1 isolates for
1097 48 h. LDH release from damaged BMDM into culture supernatant was assayed. *** $P < 0.001$
1098 by One-way ANOVA, followed by Tukey's multiple-comparison test.

1099 Fig 12. Fungal burden and cytokine production in lung after infection with Ftc555-1 as well as its
1100 isolates F5 and F6. After 60 days of infection, mice were sacrificed and (A) fungal burden in the
1101 lung were determined by CFU counting. The level of cytokines (B) IL4 (C) IL10 (D) IFN-γ (E)
1102 TNF-α in the lung were measured by ELISA. At 5-day post-infection, (F) fungal burden, and the
1103 amount of cytokines (G) IL4 (H) IL10 (I) IFN-γ (J) TNF-α in the lung were also measured. All
1104 data represent the mean of eight mice per group and errors bars are SD. * $P < 0.1$ ** $P < 0.01$. For
1105 determination of cytokine levels, one-way ANOVA with Kruskal-Wallis nonparametric test was
1106 used and followed by Bonferroni's multiple-comparison test. The t-test was used to compare the
1107 number of colony forming units (CFU) for different groups.

1108

bioRxiv preprint doi: https://doi.org/10.1101/2020.08.07.241190; this version posted August 7, 2020. The copyright holder for this preprint (which was not certified by peer review) is the author/funder, who has granted bioRxiv a license to display the preprint in perpetuity. It is made available under aCC-BY 4.0 International license.

1109 **Supporting information**

1110 S1 Table. High impact indels found in passaged Ftc555-1 isolates

1111 S1 Fig. Relative chromosome copy number of isolate H14 was obtained by qPCR.

1112 S2 Fig. Amoebae killing assay on *C. neoformans* deletion mutants. Mutants showed comparable
1113 predator zone with their parental strains.

1114 S3 Fig. Global histone H3 acetylation levels in parents and isolates. Data are means of two
1115 independent experiments with standard deviations.

1116 S4 Fig. The growth curves of Ftc555-1, F5 and F6 strains with high ($1.0x10^7$) and low ($5.0x10^3$)
1117 inoculum concentration in Sabouraud medium for seven days.

1118 S5 Fig. Cytokine production in spleen of mice after infection with Ftc555-1 as well as its isolates
1119 F5 and F6. After 60 and 5 days of infection, mice were sacrificed and the level of cytokines (A, E)
1120 IL4 (B, F) IL10 (D) IFN-γ (D, G) TNF-α in the lung were measured by ELISA. All data represent
1121 the mean of eight mice per group and errors bars are SD. For determination of cytokine levels,
1122 one-way ANOVA with Kruskal-Wallis nonparametric test was used and followed by Bonferroni's
1123 multiple-comparison test. The t-test was used to compare the number of colony forming units
1124 (CFU) for different groups.

1125 S6 Fig. Virulence of parents and variant isolates in the *G. mellonella* larvae infection model. The
1126 Kaplan-Meier plots shows the survival of *G. mellonella* after injection of cryptococcal cells ($10^3$
1127 cells/larva).

1128 S7 Fig. Summary of phenotypic changes occurred in amoeba-passaged isolates

1129 S1 Movie. Time-lapse imaging showing nuclear division of pseudohyphae.

# Figure 1

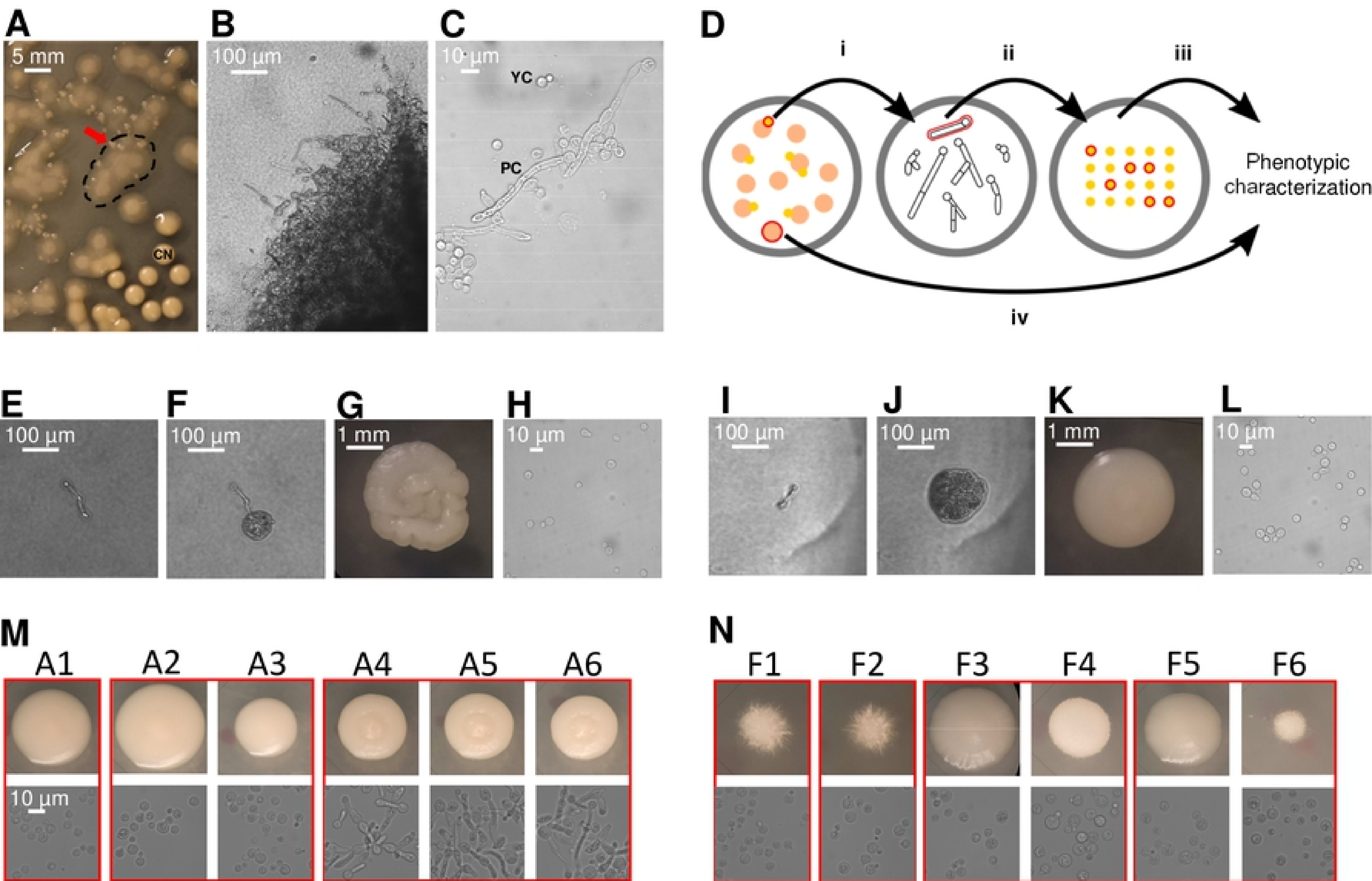


Figure 1

# Figure 2

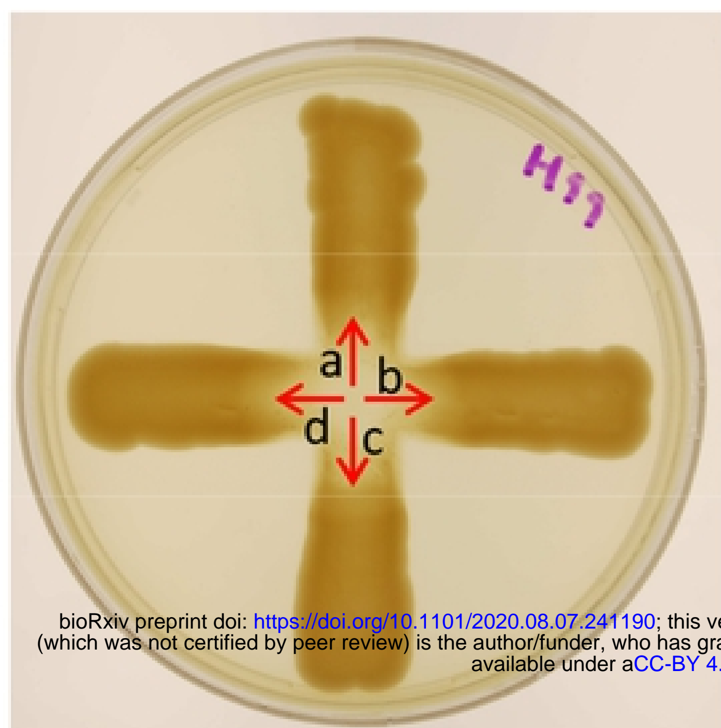


bioRxiv preprint doi: https://doi.org/10.1101/2020.08.07.241190; this version posted August 7, 2020. The copyright holder for this preprint (which was not certified by peer review) is the author/funder, who has granted bioRxiv a license to display the preprint in perpetuity. It is made available under aCC-BY 4.0 International license.

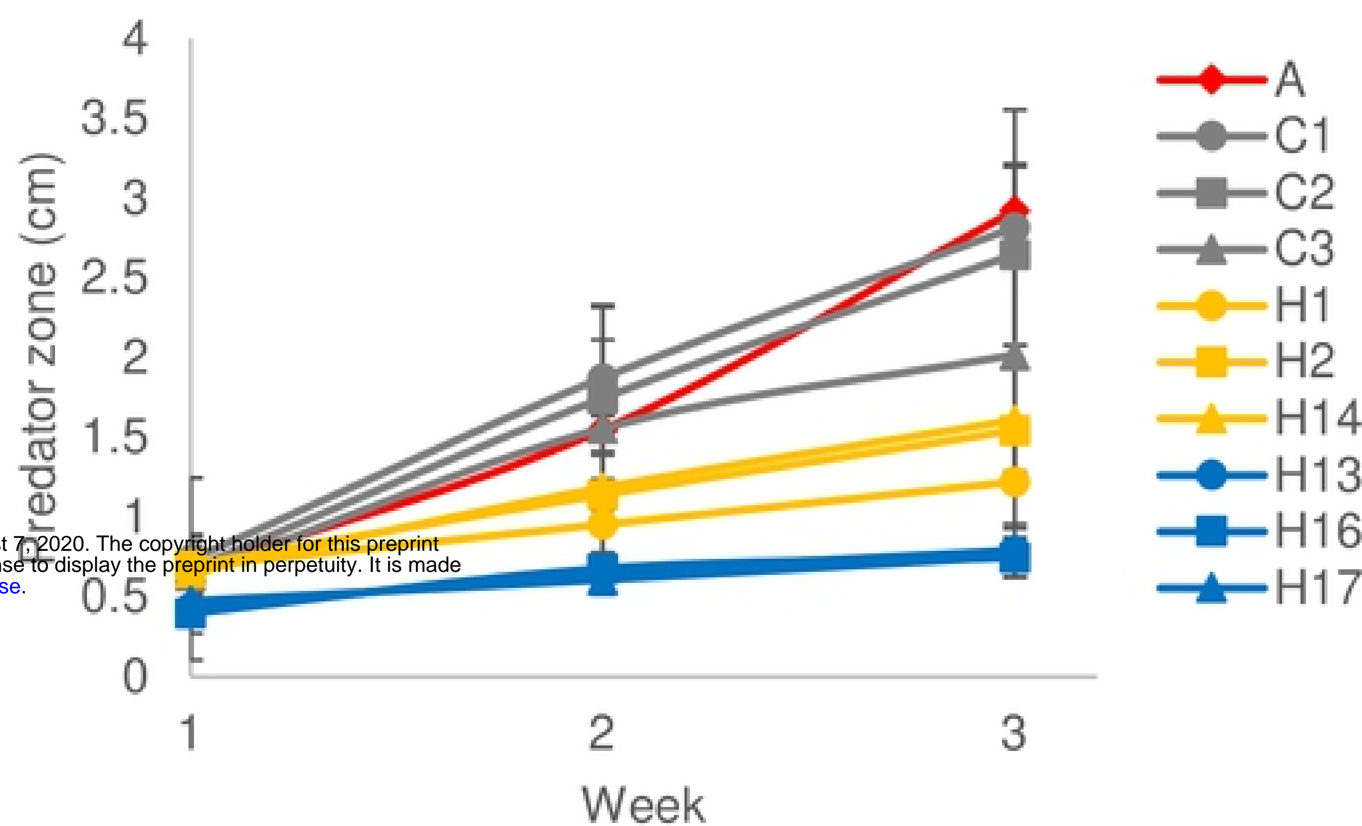


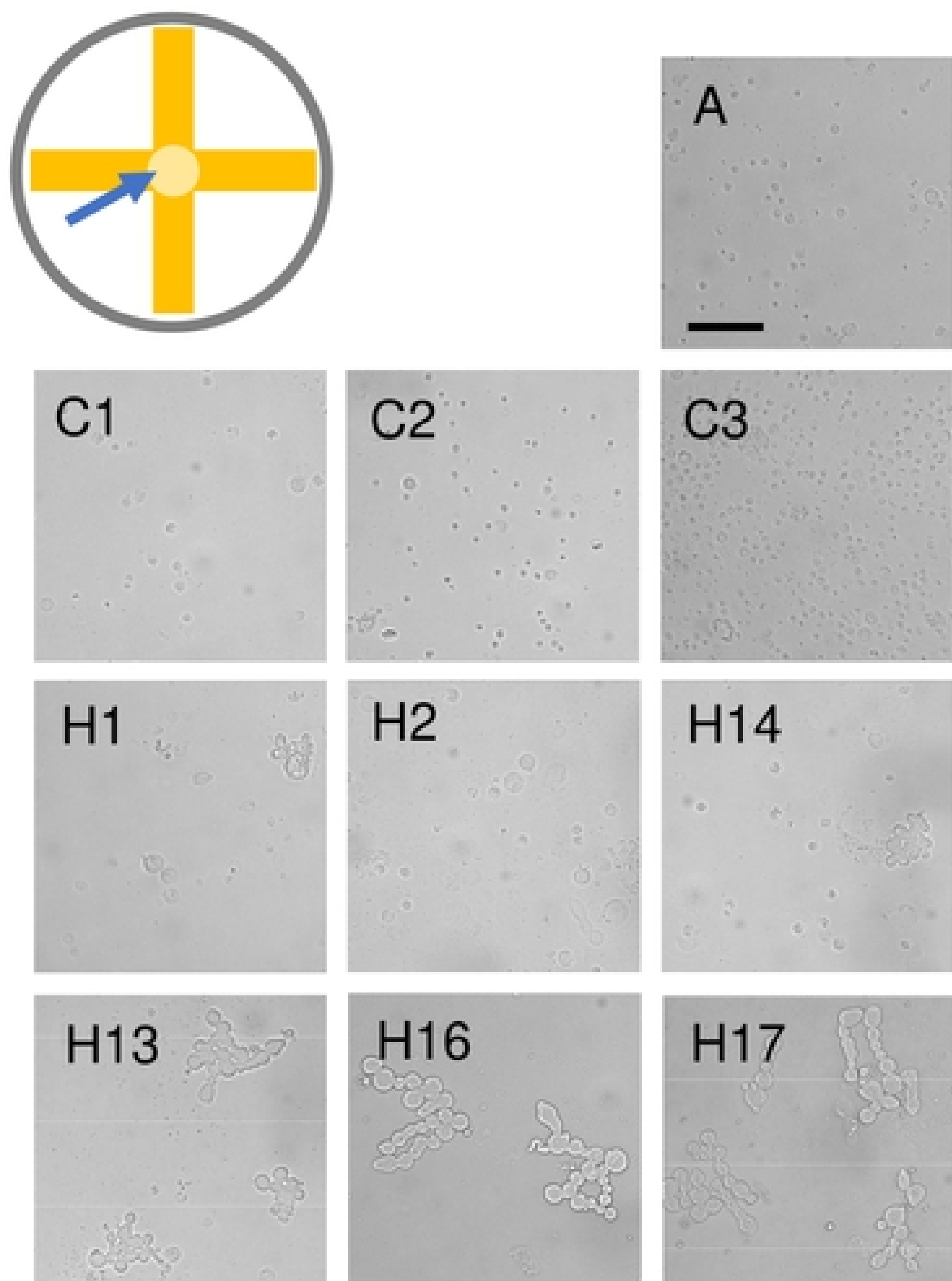


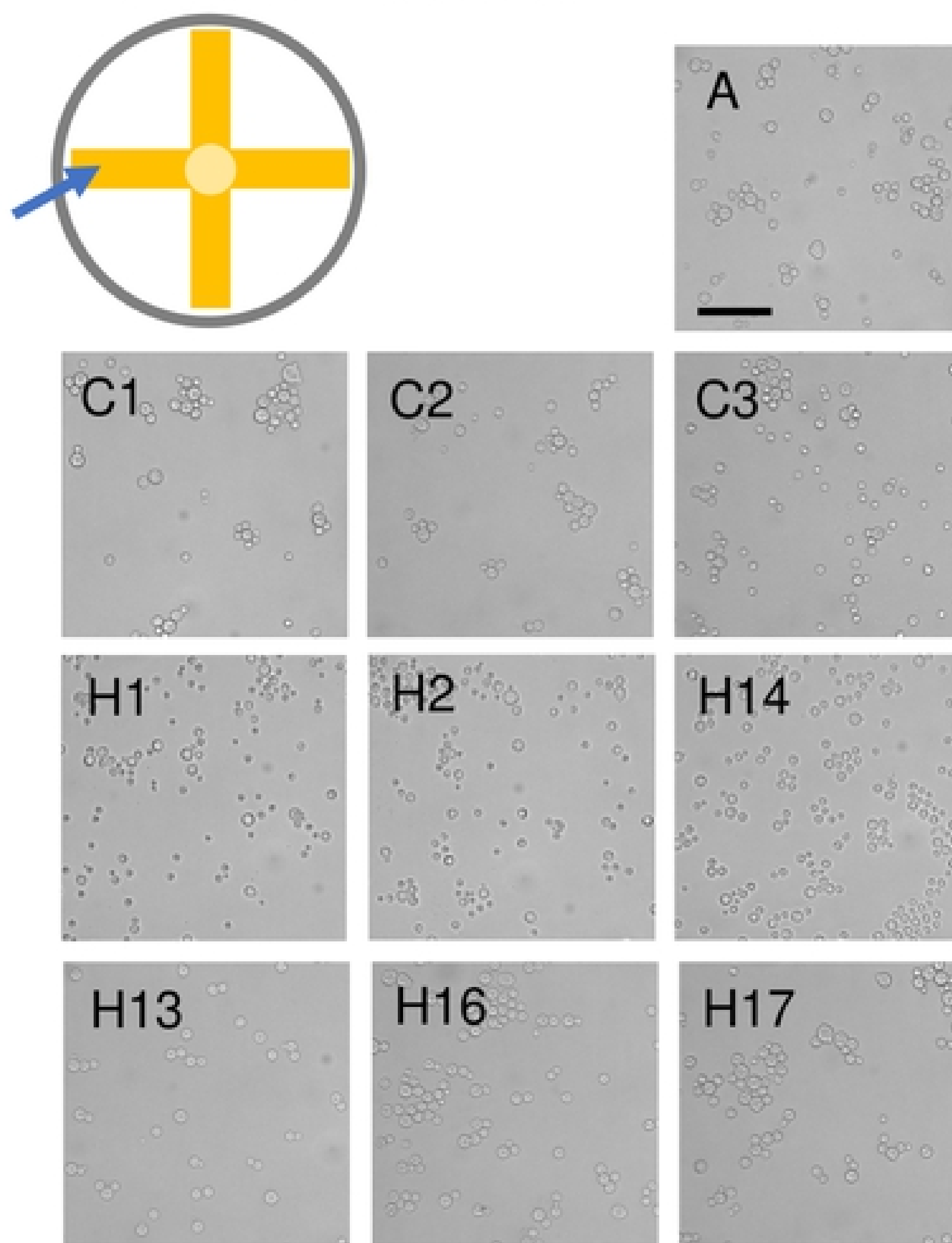


Figure 2

Figure 3

bioRxiv preprint doi: https://doi.org/10.1101/2020.08.07.241190; this version posted August 7, 2020. The copyright holder for this preprint (which was not certified by peer review) is the author/funder, who has granted bioRxiv a license to display the preprint in perpetuity. It is made available under aCC-BY 4.0 International license.

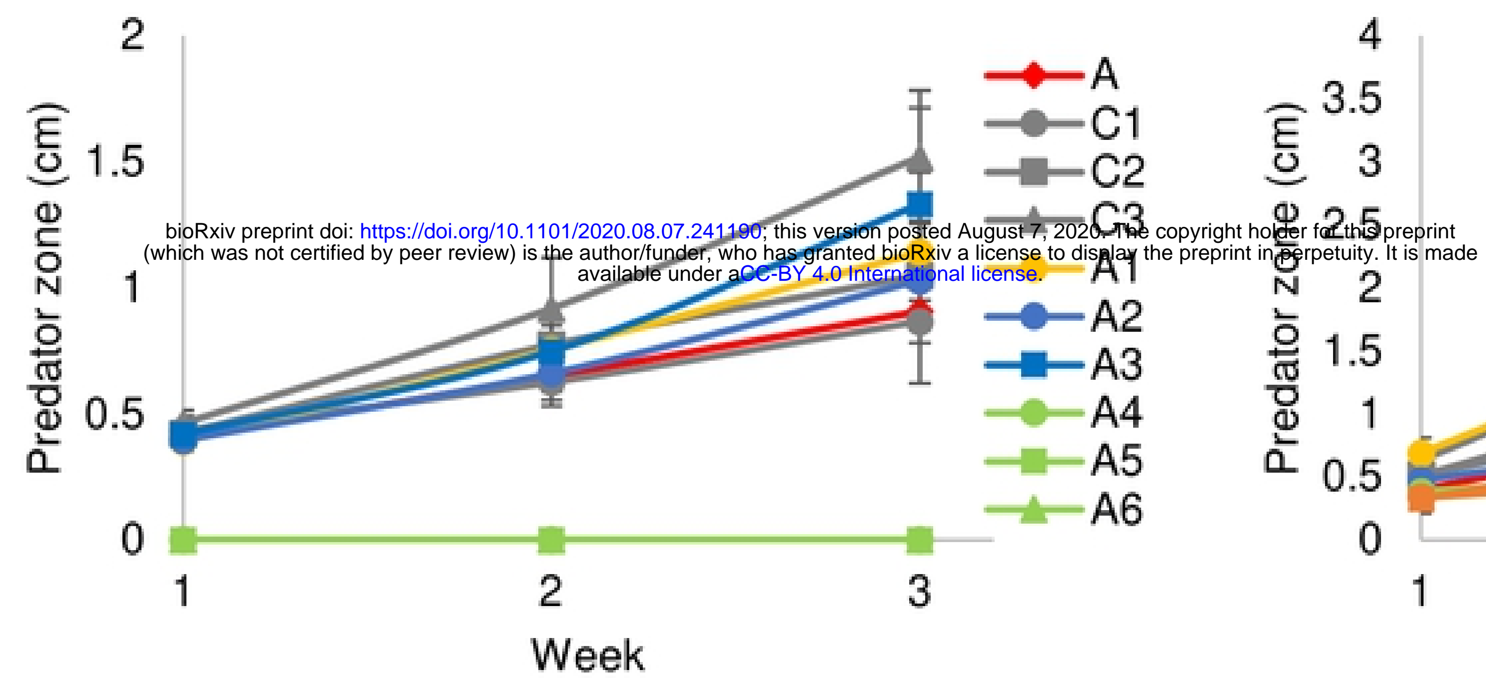


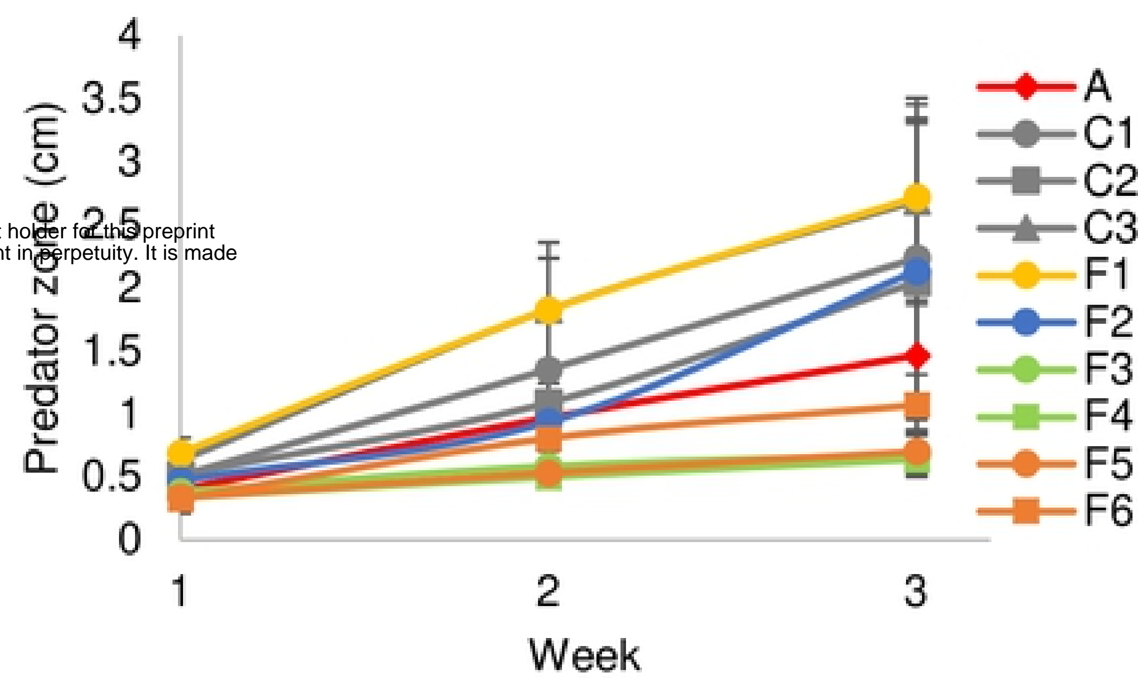


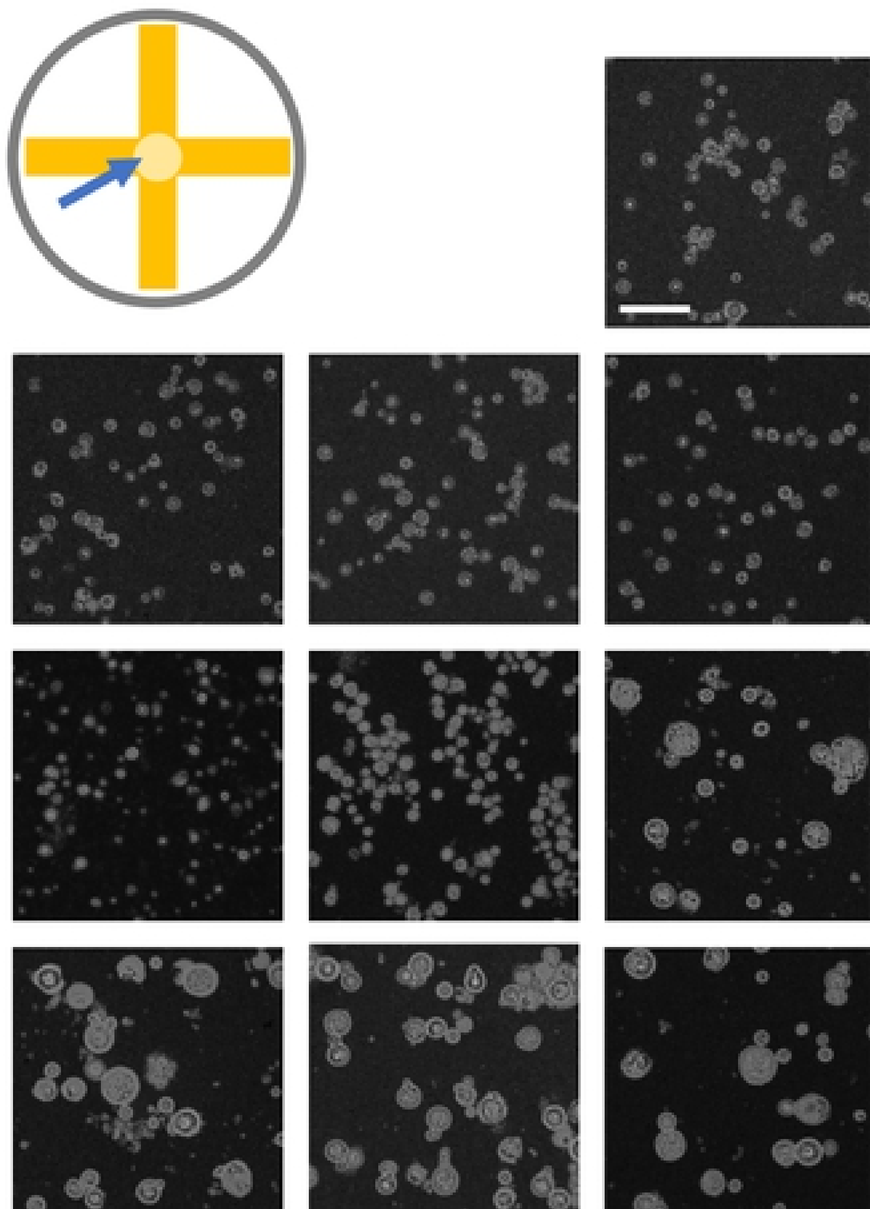


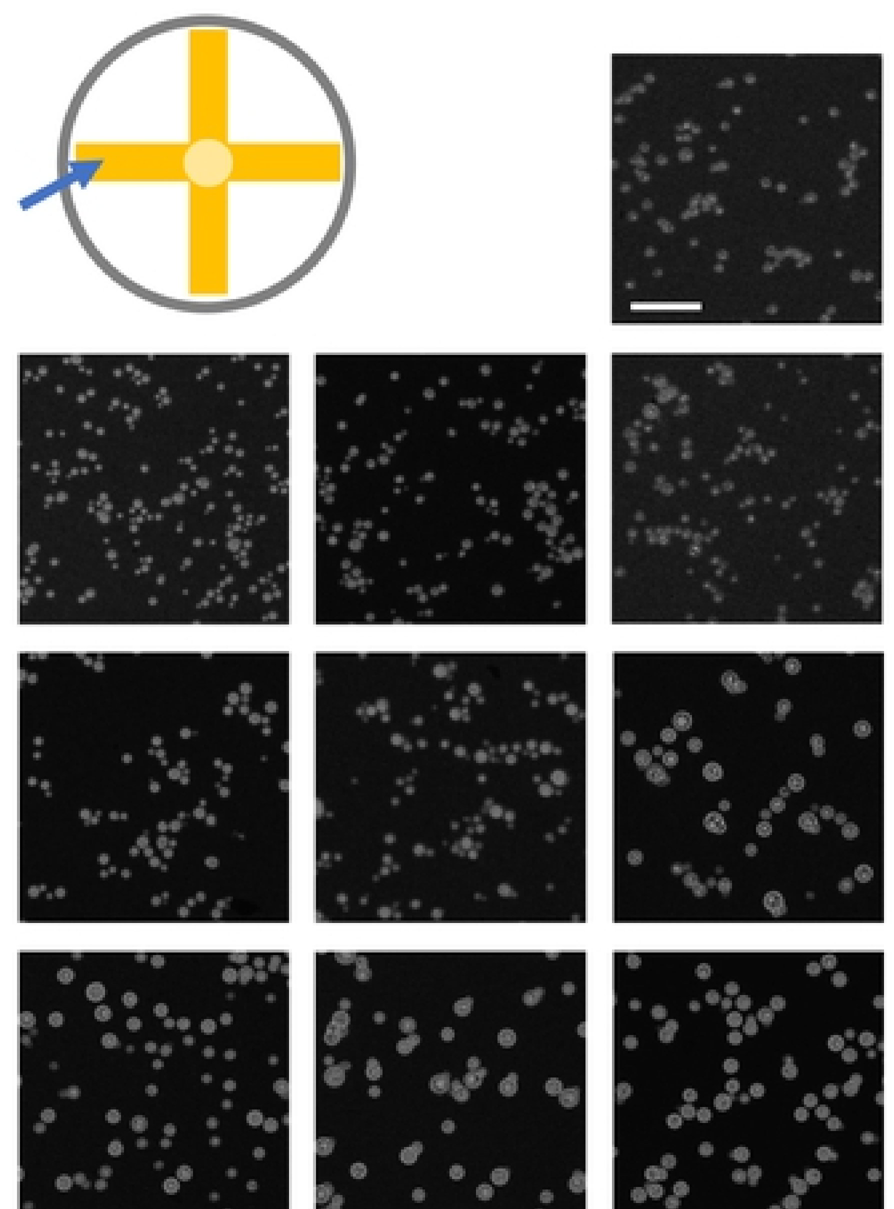


Figure 3

# Figure 4

**A**

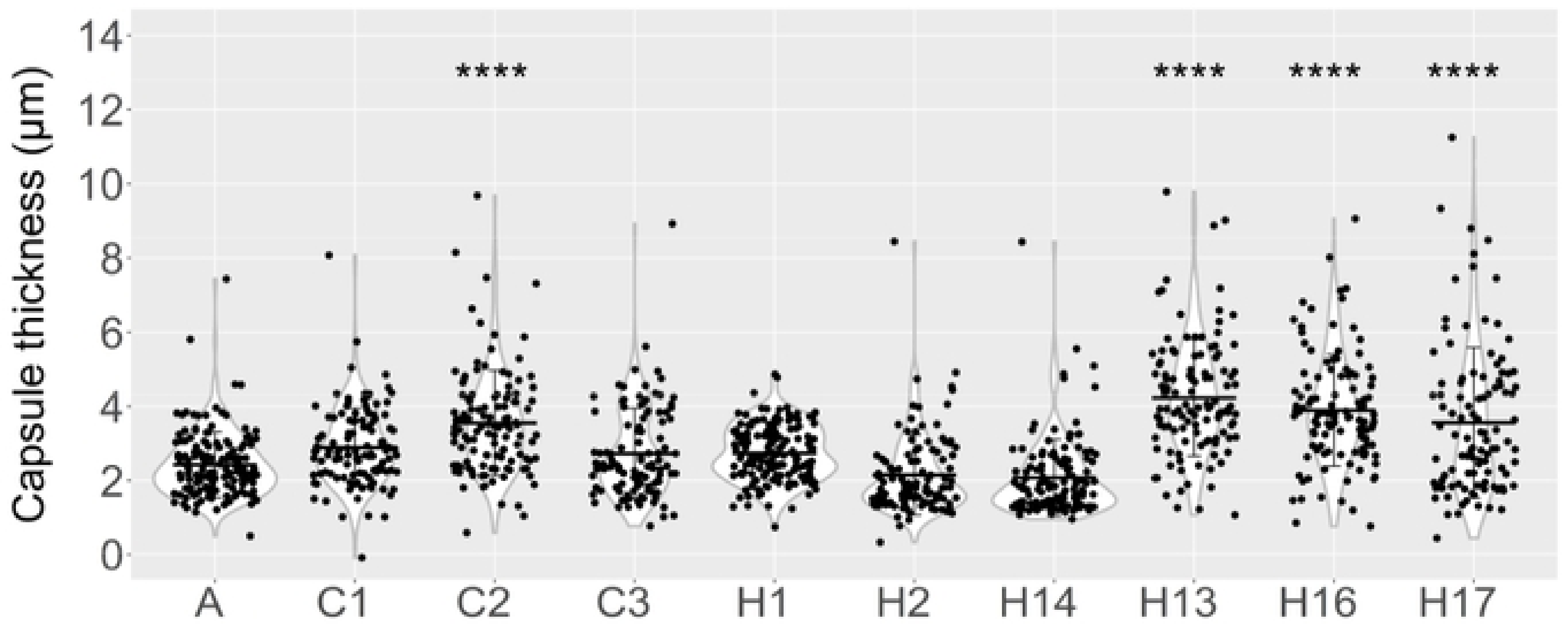


bioRxiv preprint doi: https://doi.org/10.1101/2020.08.07.241190; this version posted August 7, 2020. The copyright holder for this preprint (which was not certified by peer review) is the author/funder, who has granted bioRxiv a license to display the preprint in perpetuity. It is made available under aCC-BY 4.0 International license.

**B**

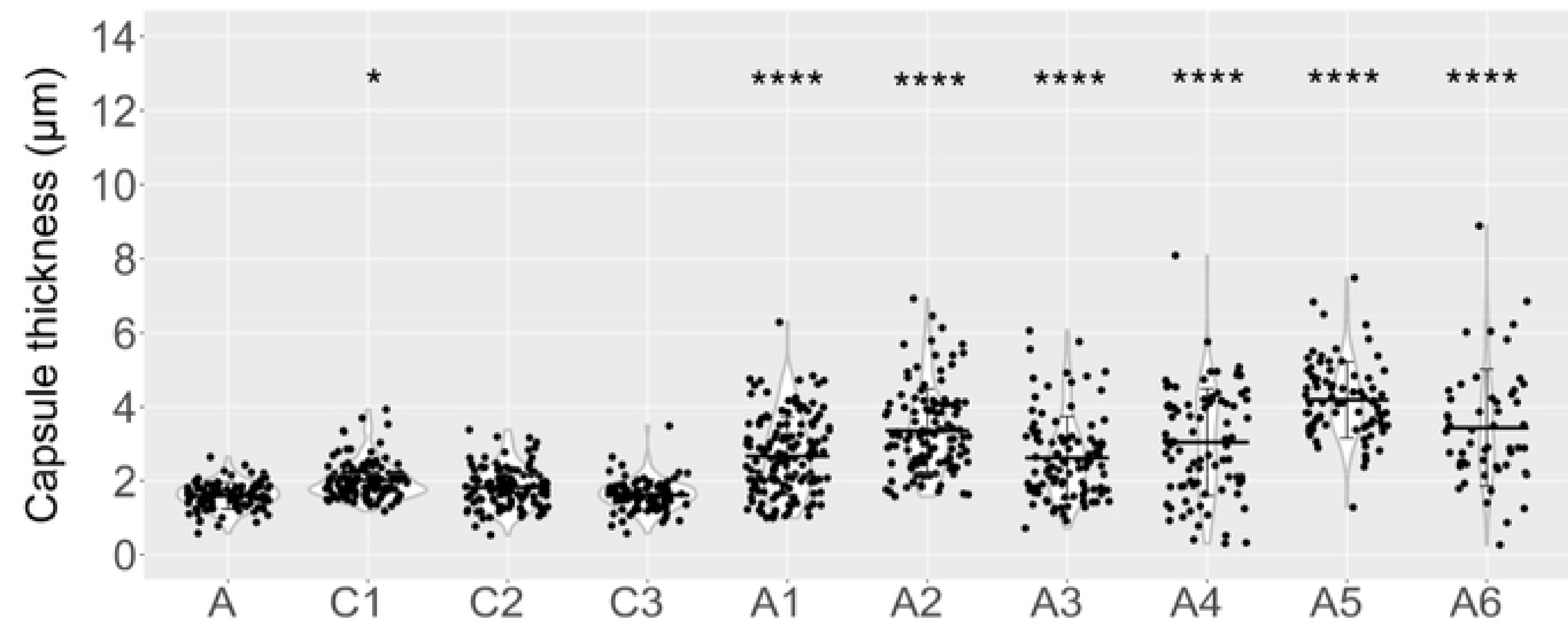


**C**

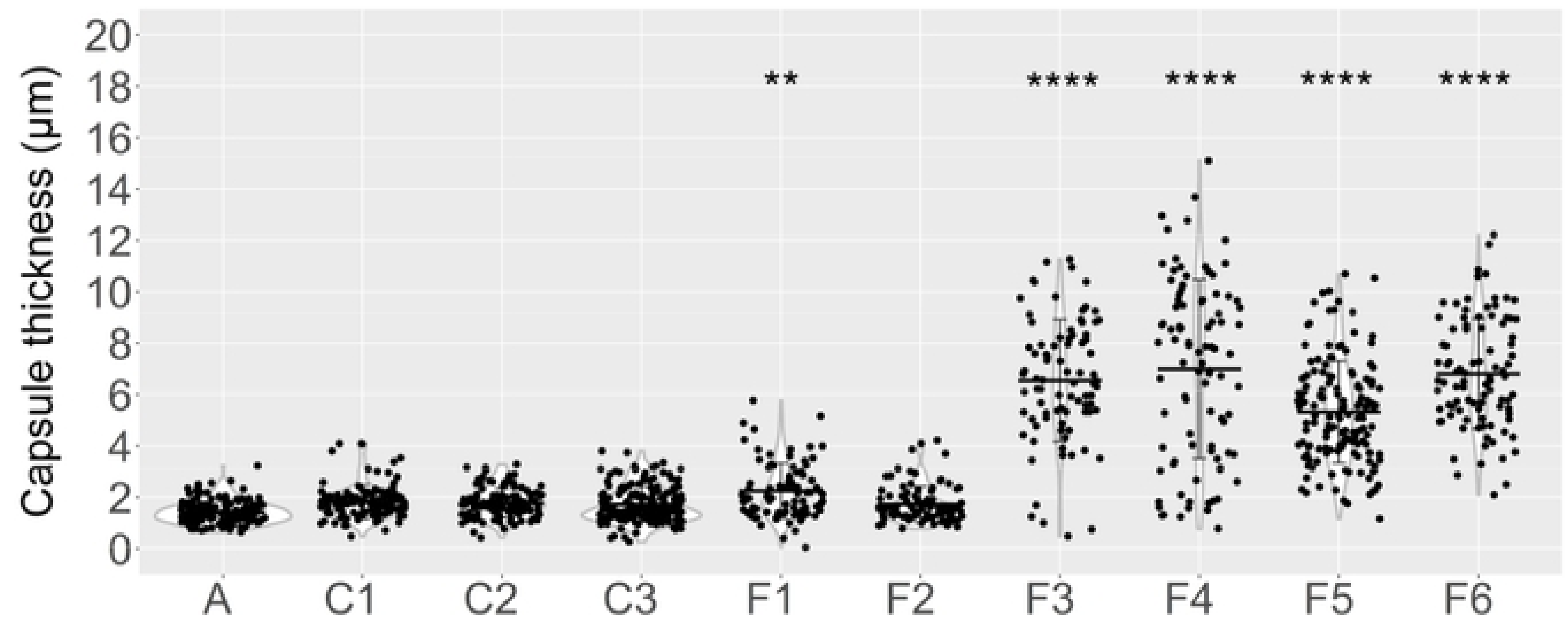


Figure 4

Figure 5

bioRxiv preprint doi: https://doi.org/10.1101/2020.08.07.241190; this version posted August 7, 2020. The copyright holder for this preprint (which was not certified by peer review) is the author/funder, who has granted bioRxiv a license to display the preprint in perpetuity. It is made available under aCC-BY 4.0 International license.

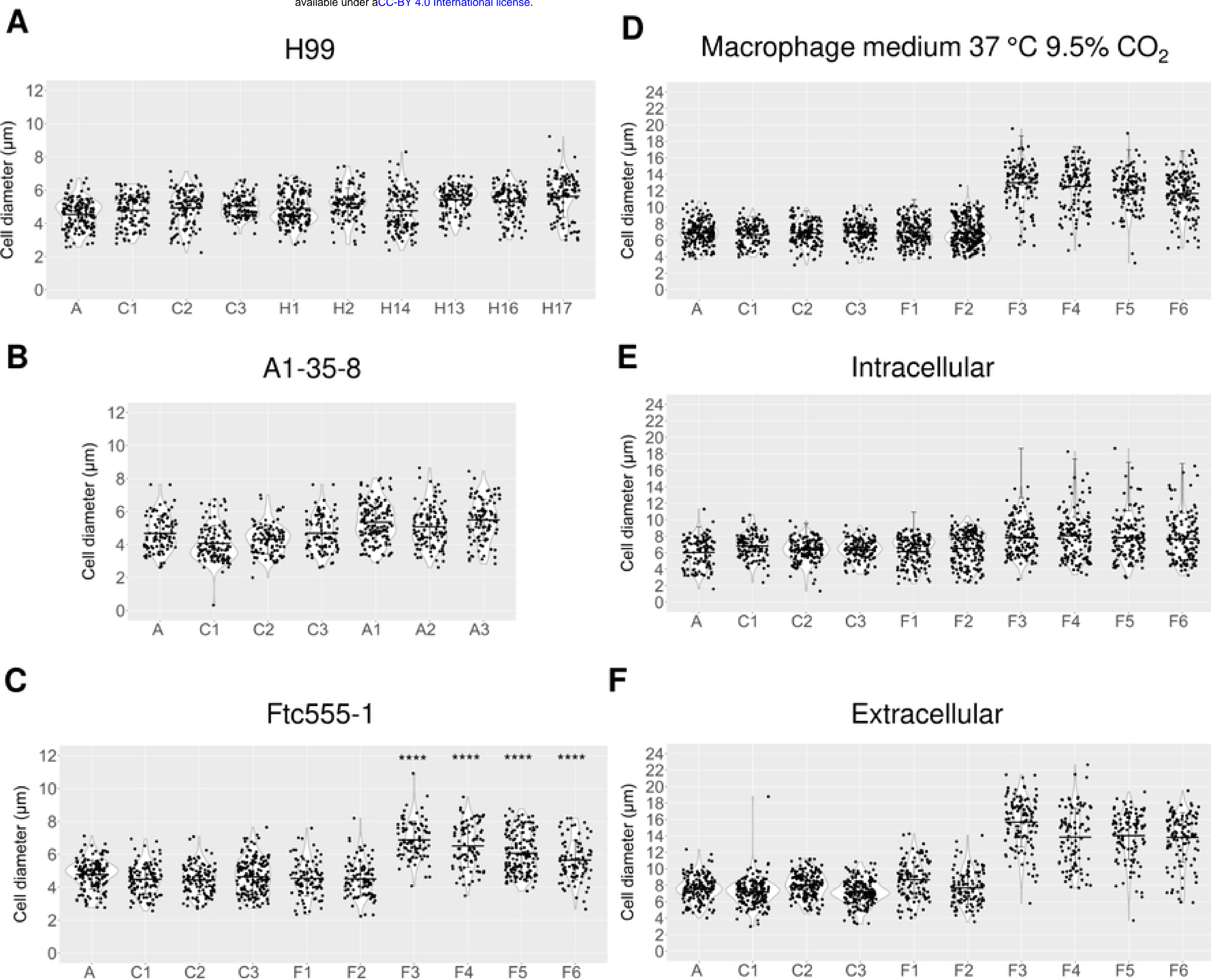


Figure 5

# Figure 6

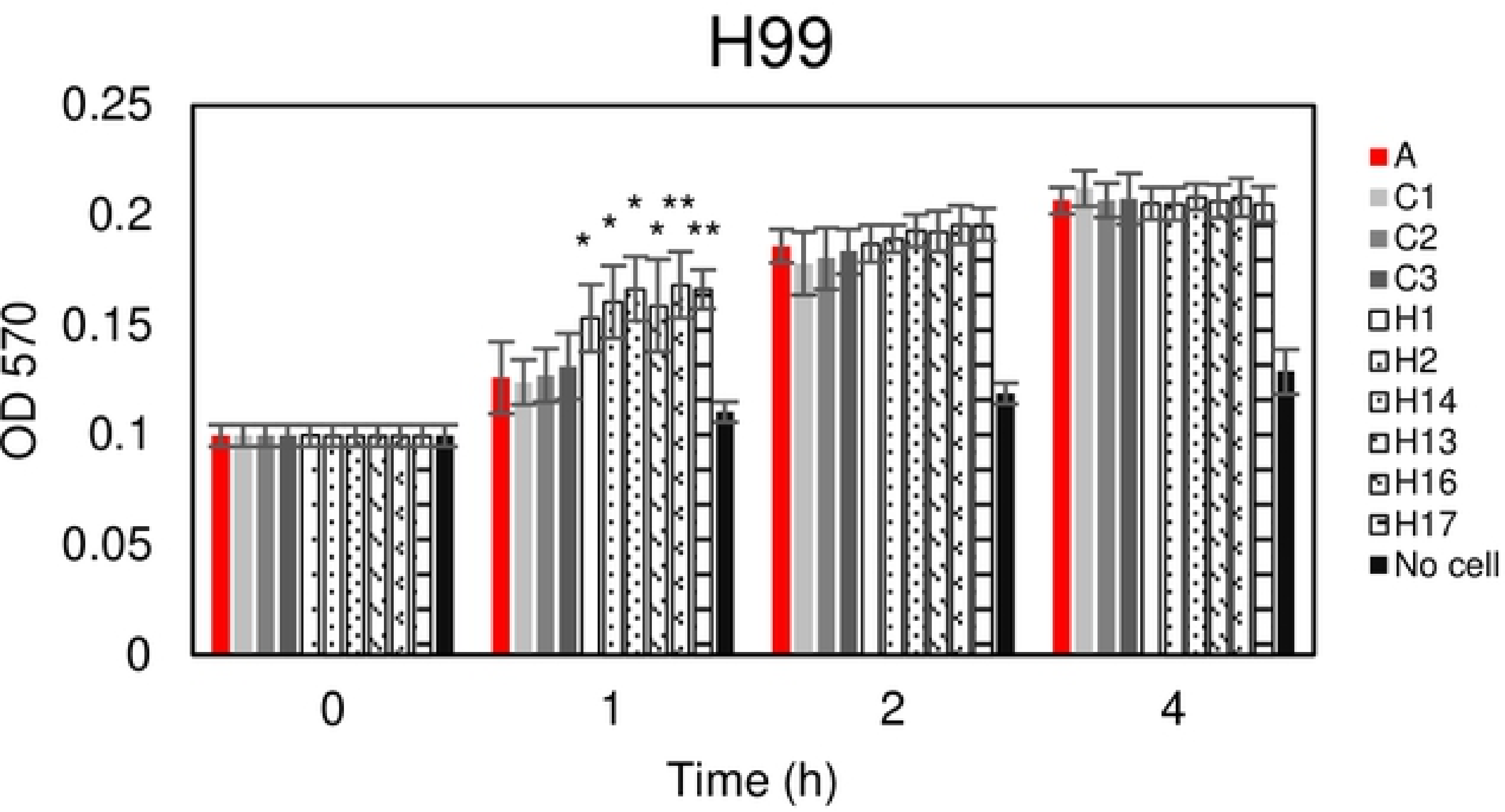


bioRxiv preprint doi: https://doi.org/10.1101/2020.08.07.241190; this version posted August 7, 2020. The copyright holder for this preprint (which was not certified by peer review) is the author/funder, who has granted bioRxiv a license to display the preprint in perpetuity. It is made available under aCC-BY 4.0 International license.

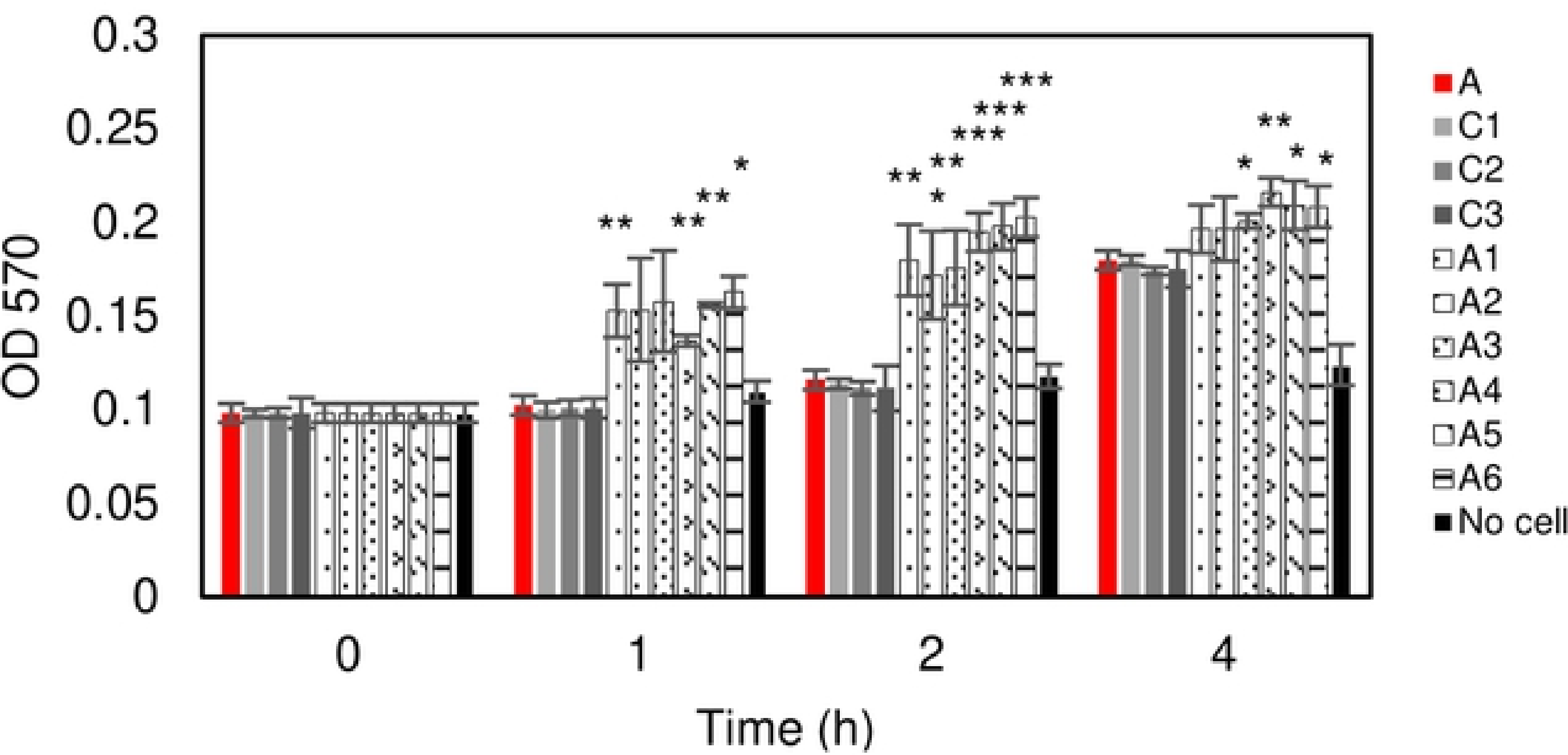


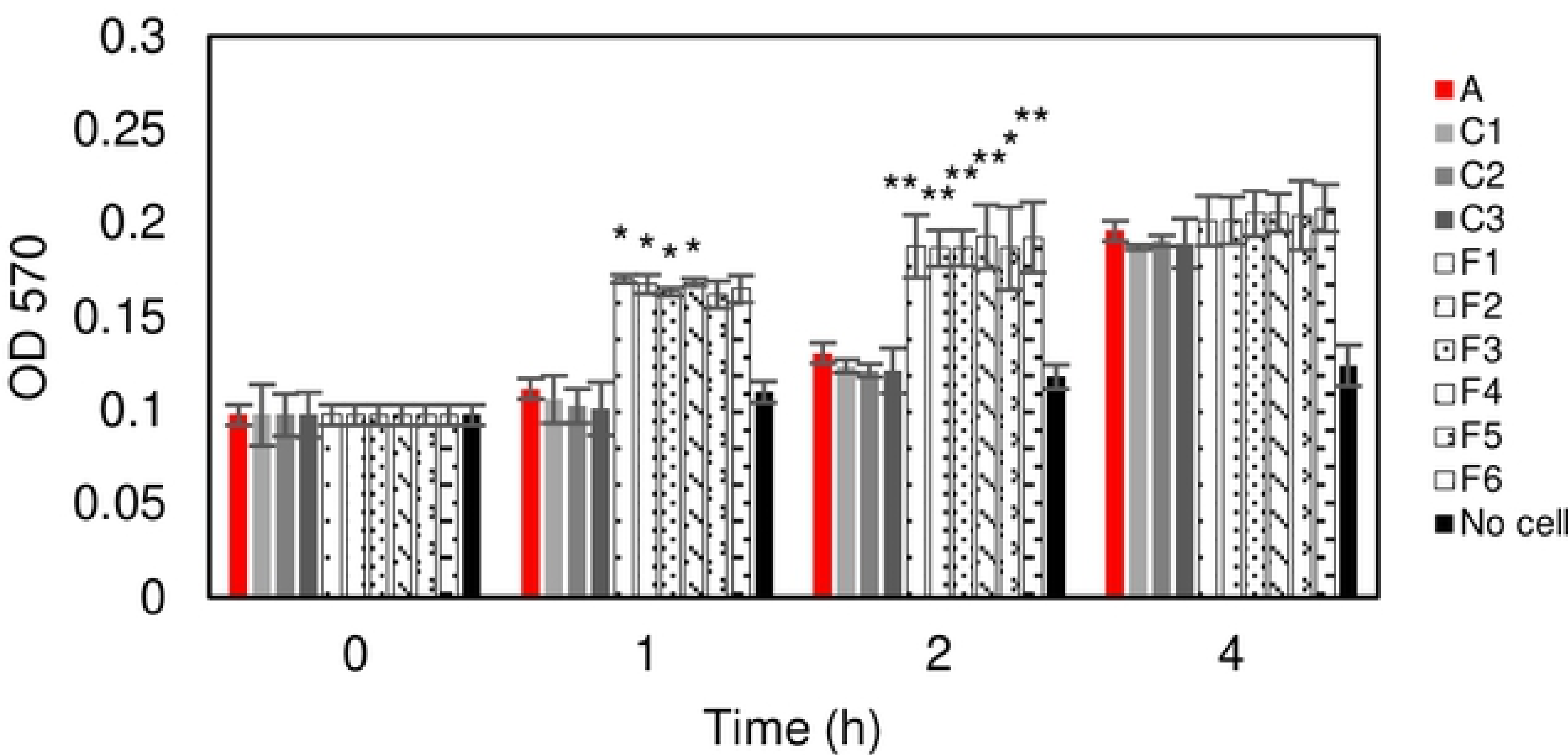


Figure 6

# Figure 7

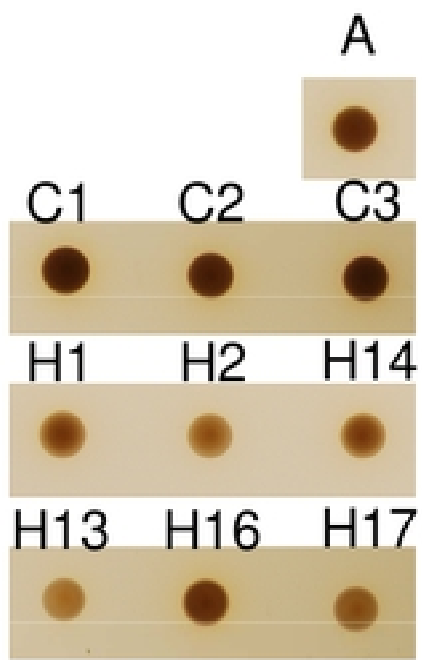


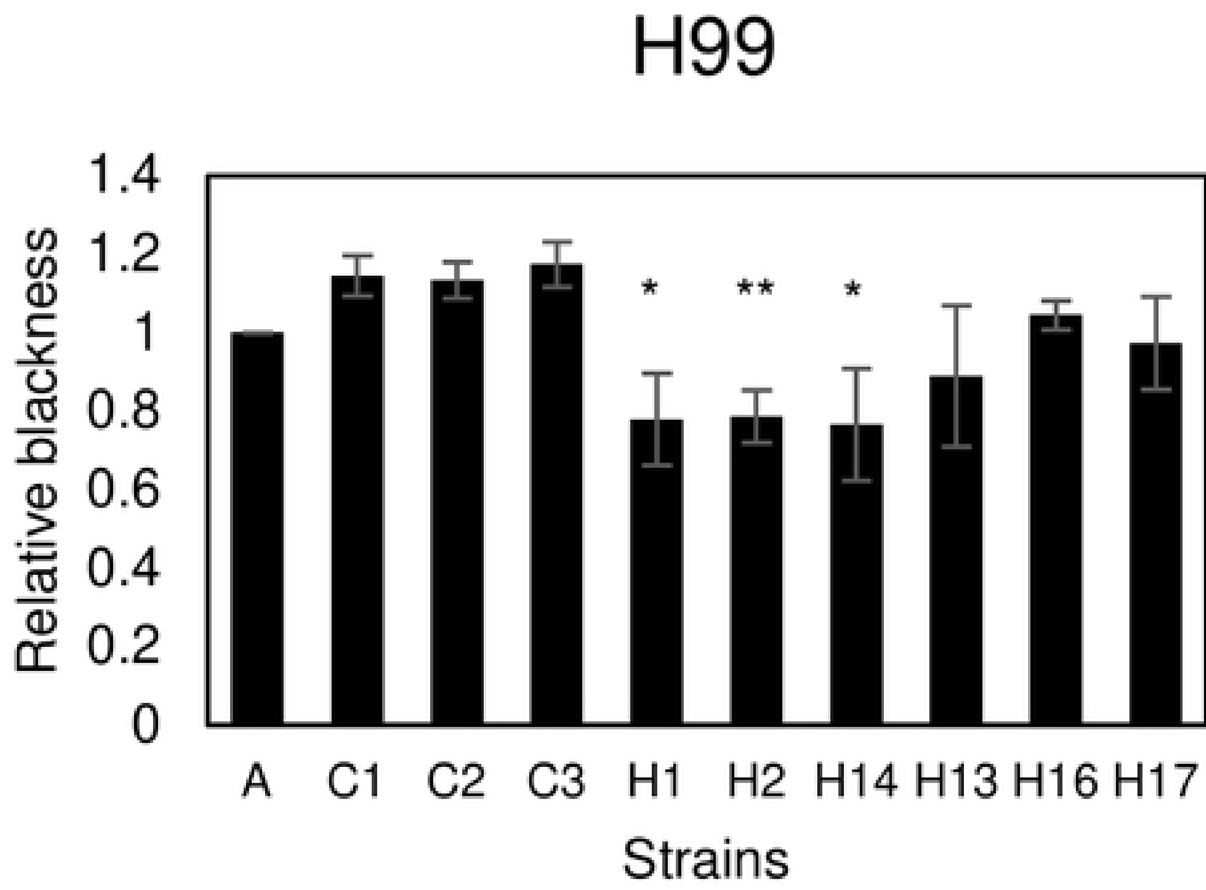


bioRxiv preprint doi: https://doi.org/10.1101/2020.08.07.241190; this version posted August 7, 2020. The copyright holder for this preprint (which was not certified by peer review) is the author/funder, who has granted bioRxiv a license to display the preprint in perpetuity. It is made available under aCC-BY 4.0 International license.

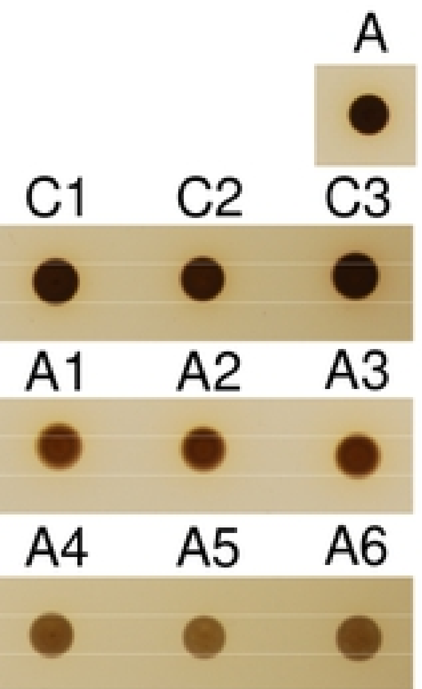


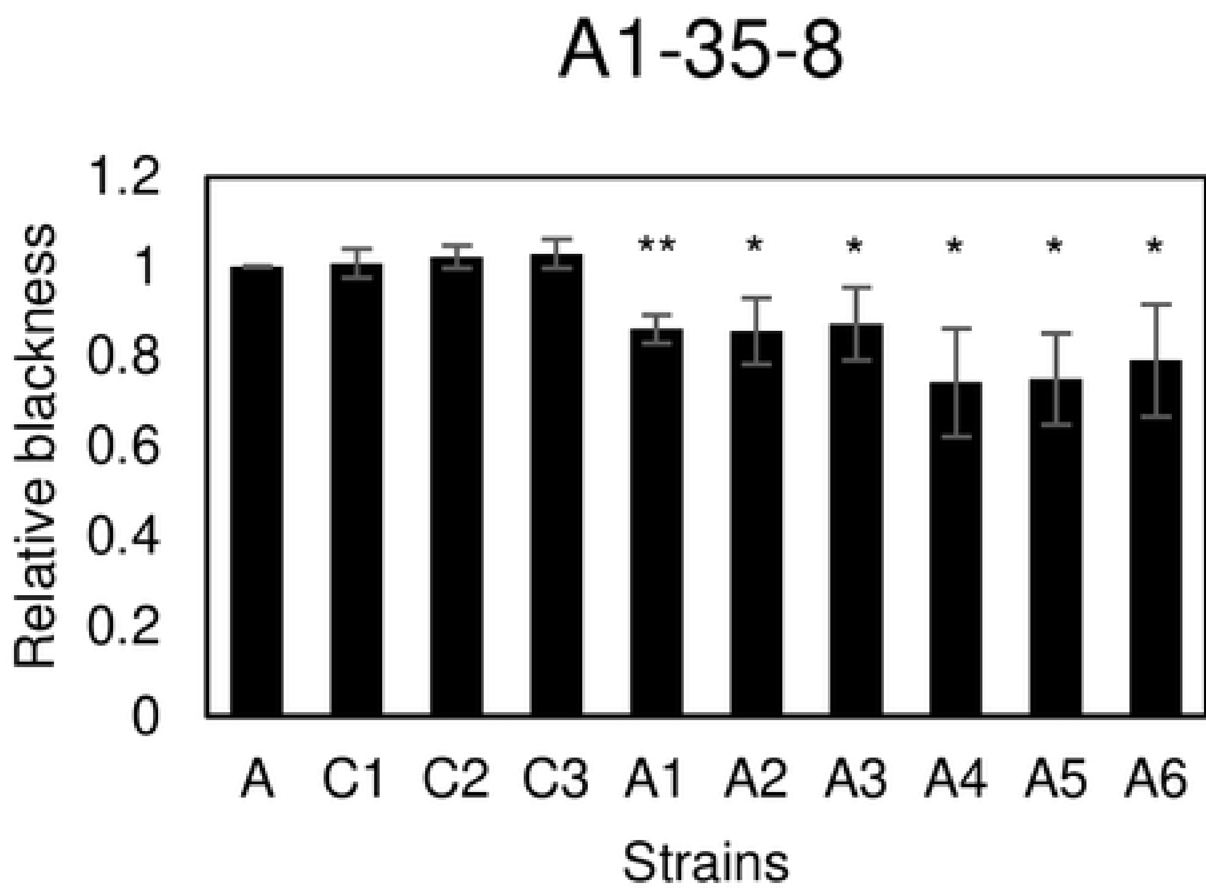


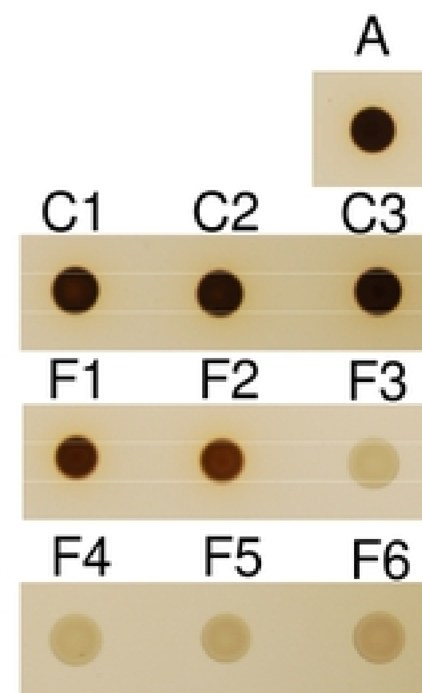


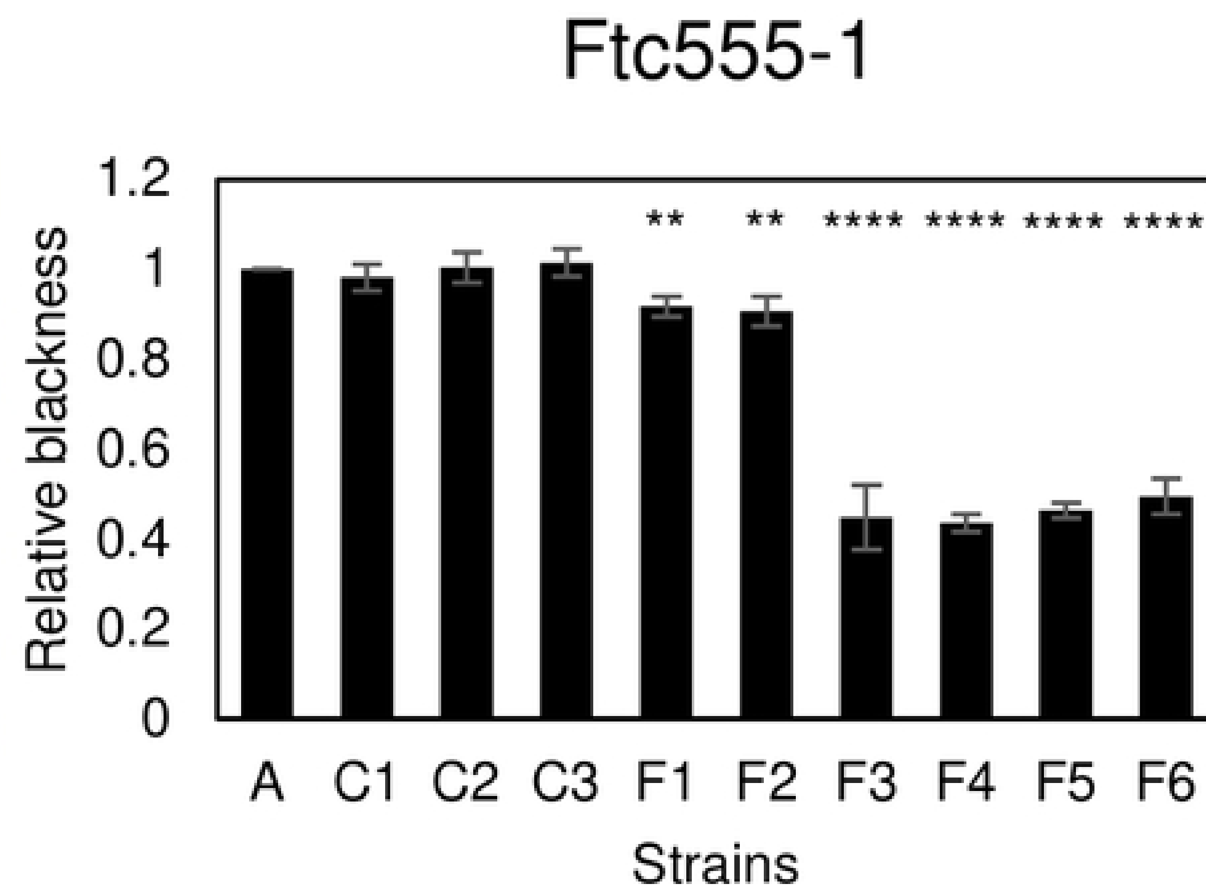


Figure 7

# Figure 8

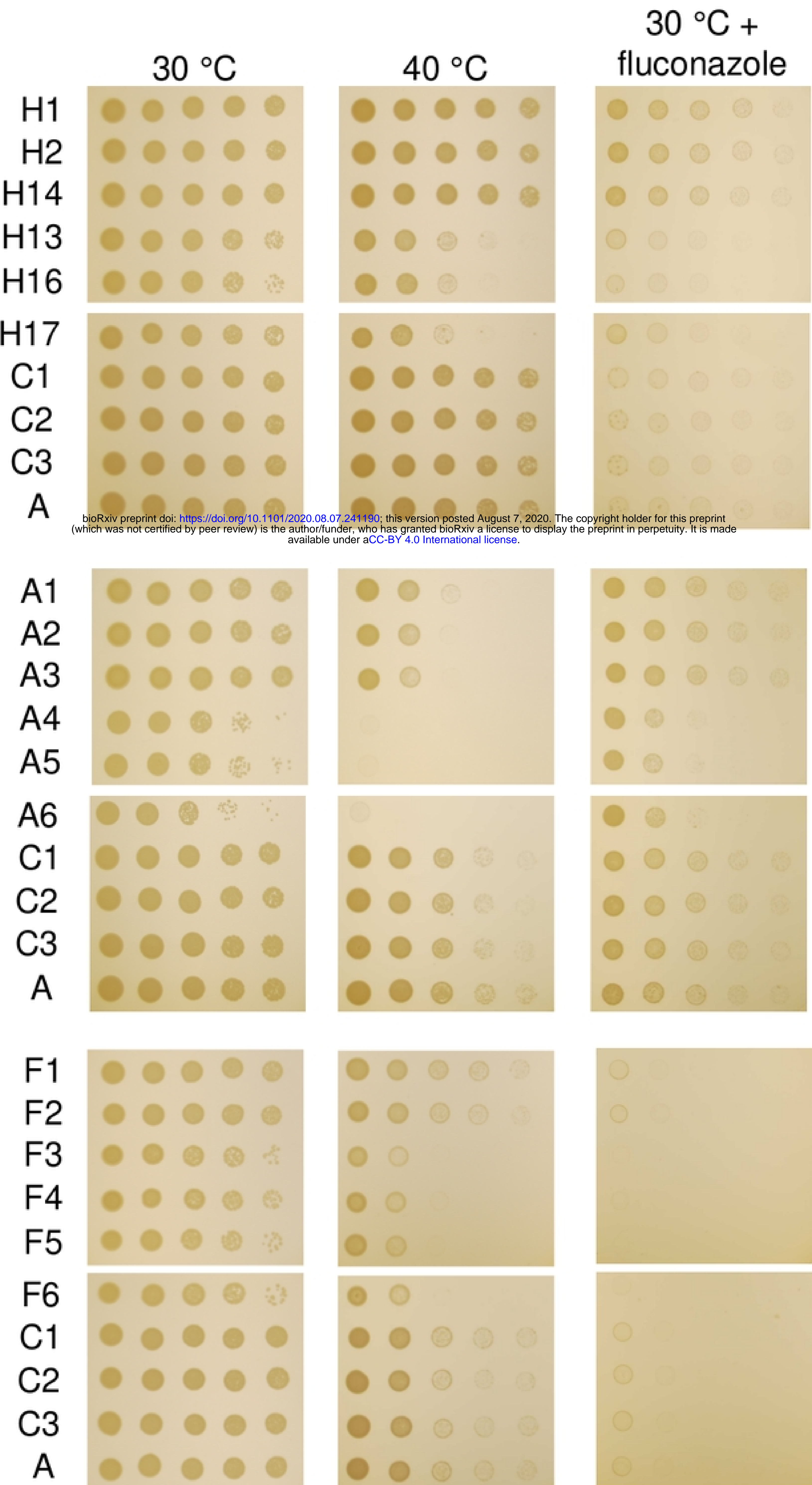


bioRxiv preprint doi: https://doi.org/10.1101/2020.08.07.241190; this version posted August 7, 2020. The copyright holder for this preprint (which was not certified by peer review) is the author/funder, who has granted bioRxiv a license to display the preprint in perpetuity. It is made available under aCC-BY 4.0 International license.

Figure 8

Figure 9

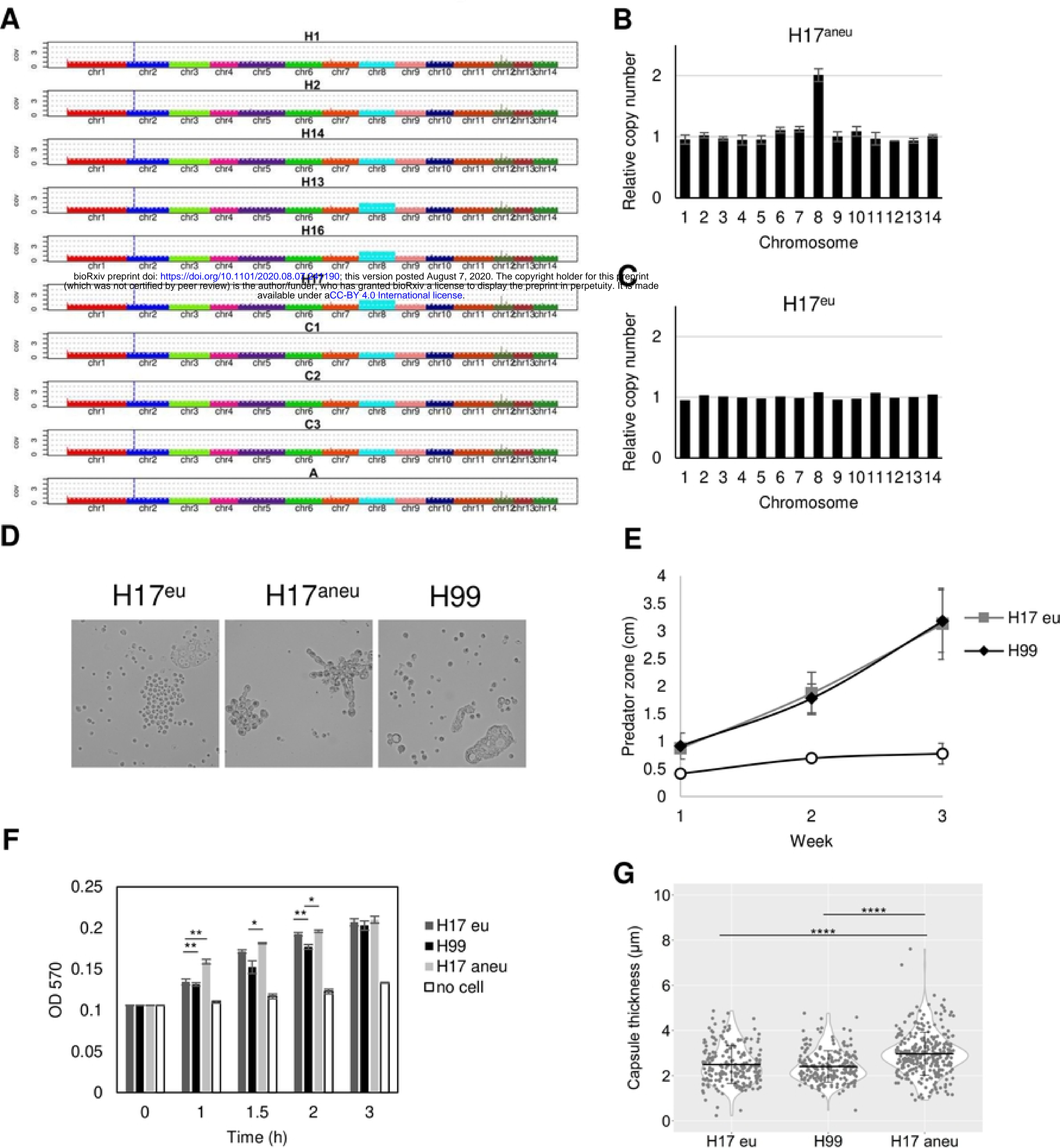


bioRxiv preprint doi: https://doi.org/10.1101/2020.08.07.241190; this version posted August 7, 2020. The copyright holder for this preprint (which was not certified by peer review) is the author/funder, who has granted bioRxiv a license to display the preprint in perpetuity. It is made available under aCC-BY 4.0 International license.

Figure 9

Figure 10

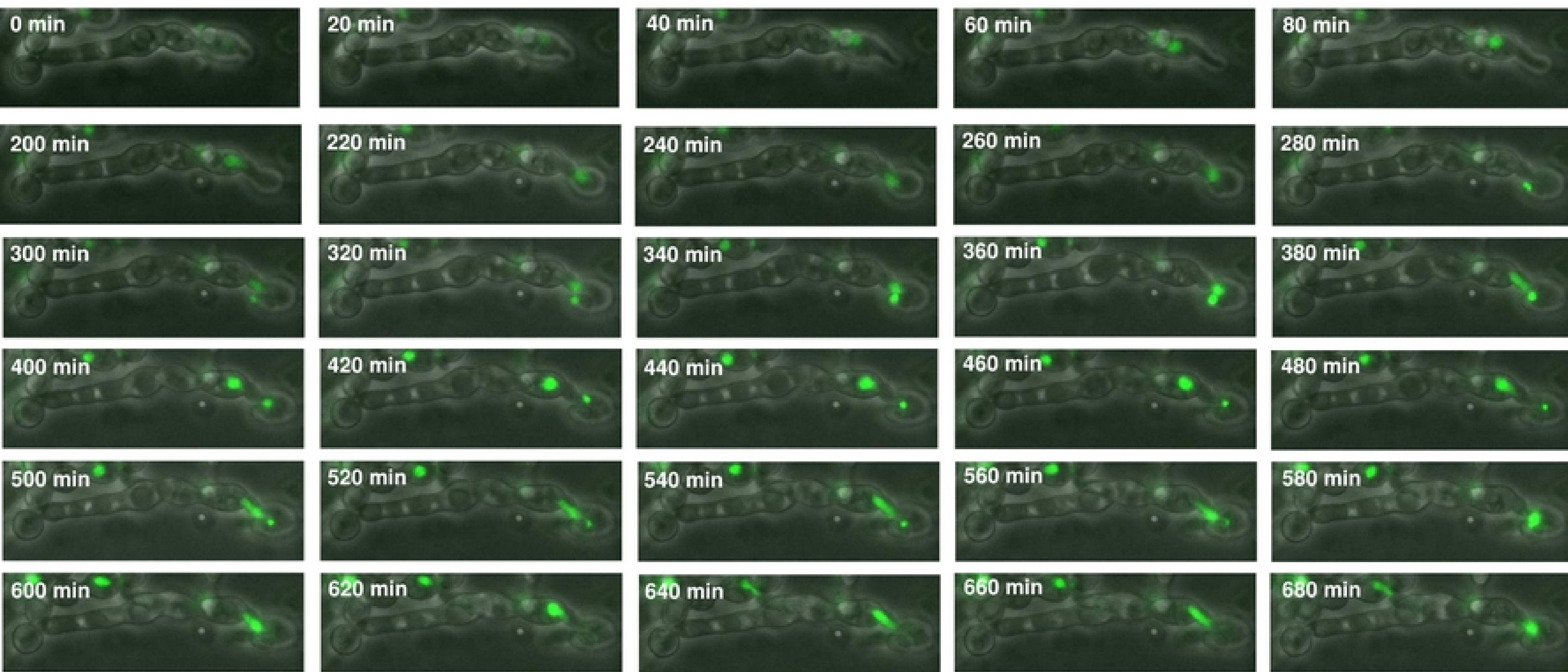


Figure 10

Figure 11

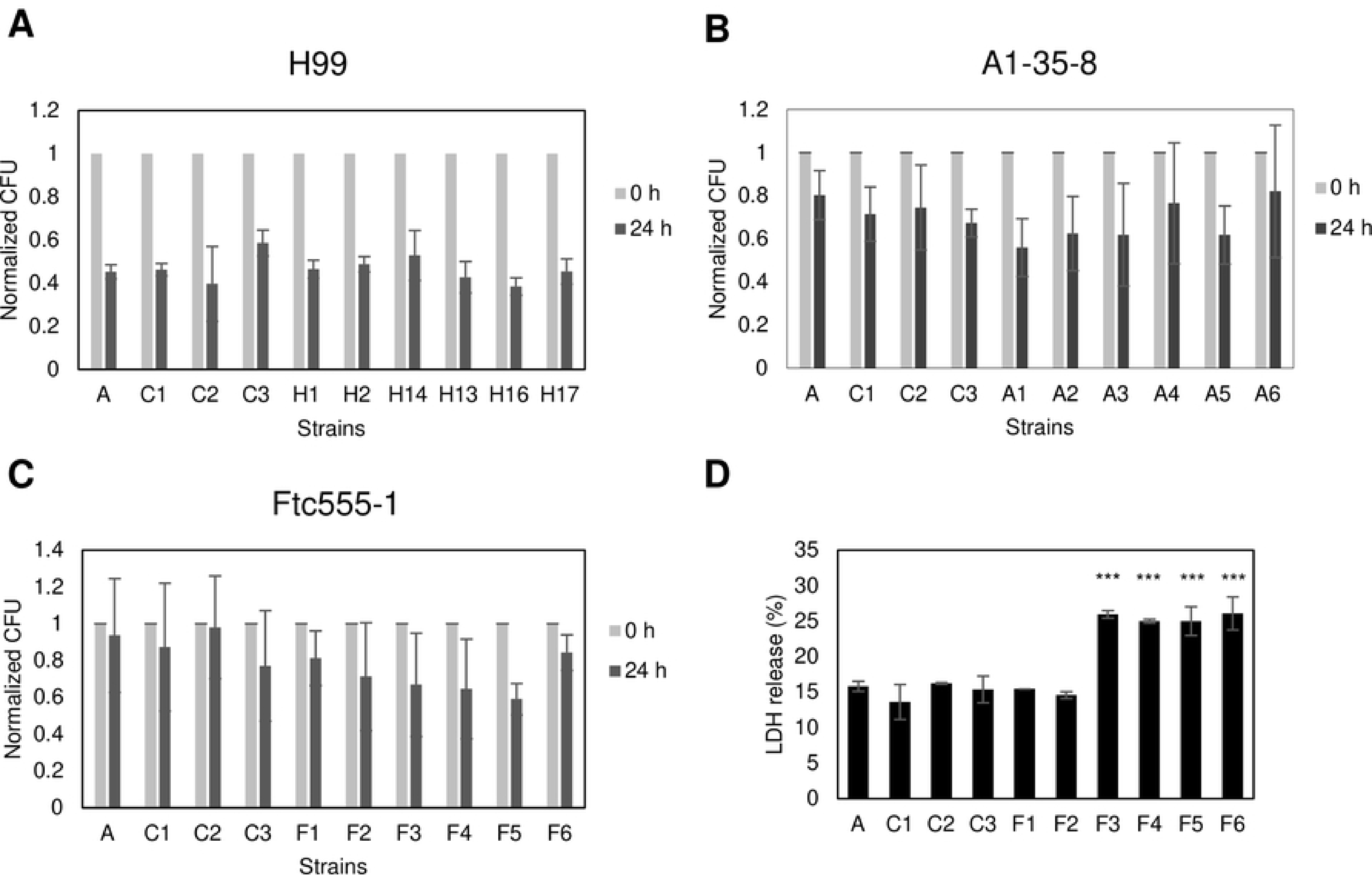


Figure 11

Figure 12

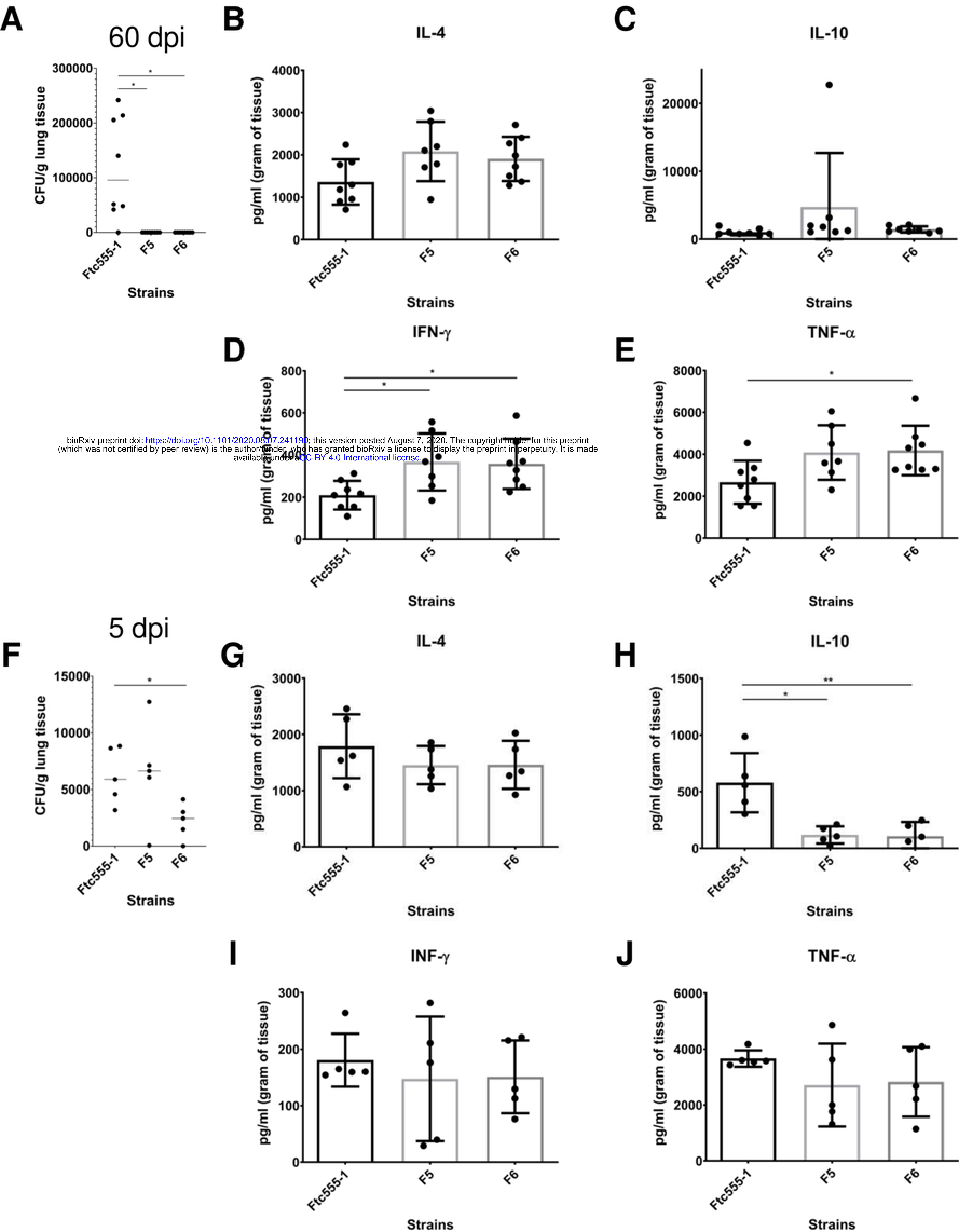


bioRxiv preprint doi: https://doi.org/10.1101/2020.08.07.241190; this version posted August 7, 2020. The copyright holder for this preprint (which was not certified by peer review) is the author/funder, who has granted bioRxiv a license to display the preprint in perpetuity. It is made available under aCC-BY 4.0 International license.

Figure 12